JGR Atmospheres

RESEARCH ARTICLE
10.1029/2021JD034679

Estimation of Possible Primary Biological Particle Emissions and Rupture Events at the Southern Great Plains ARM Site

Tamanna Subba[1], **Michael J. Lawler**[2,3], **and Allison L. Steiner**[1]

[1]Department of Climate and Space Sciences and Engineering, University of Michigan, Ann Arbor, MI, USA, [2]Department of Chemistry, University of California, Irvine, Irvine, CA, USA, [3]Now at Chemical Sciences Laboratory, CIRES, University of Colorado, Boulder, Boulder, CO, USA

Key Points:

- An average of 12 days per year are estimated as primary pollen event days with high interannual variability
- During primary pollen events with precipitation or high humidity, rupture events are indicated during ~4 days per year
- During or after the prolonged exposure of rainfall for >10 h, ~20 days per year show evidence of fungal spore rupture events

Supporting Information:

Supporting Information may be found in the online version of this article.

Correspondence to:

T. Subba,
tsubba@umich.edu

Citation:

Subba, T., Lawler, M. J., & Steiner, A. L. (2021). Estimation of possible primary biological particle emissions and rupture events at the Southern Great Plains ARM site. *Journal of Geophysical Research: Atmospheres*, *126*, e2021JD034679. https://doi.org/10.1029/2021JD034679

Received 28 JAN 2021
Accepted 26 JUL 2021

Author Contributions:

Conceptualization: Tamanna Subba, Allison L. Steiner
Data curation: Tamanna Subba, Michael J. Lawler
Formal analysis: Tamanna Subba, Michael J. Lawler
Funding acquisition: Allison L. Steiner
Investigation: Tamanna Subba, Allison L. Steiner
Methodology: Tamanna Subba, Michael J. Lawler, Allison L. Steiner
Project Administration: Allison L. Steiner
Resources: Michael J. Lawler, Allison L. Steiner
Software: Tamanna Subba, Michael J. Lawler
Supervision: Allison L. Steiner

Abstract We use 10 years of data from the Department of Energy (DoE) Atmospheric Radiation Measurements (ARM) United States Southern Great Plains (SGP) site with nearby regional pollen and fungal spore measurements to indirectly estimate the seasonal influence of these two primary biological aerosol particles (PBAP). We estimate possible primary emissions of larger PBAP and PBAP rupture events, which form submicron organic aerosol during precipitation or high relative humidity. High pollen counts at two urban stations near SGP occur during late winter/early spring (day of year (DOY) 50–120) and late summer (DOY 240–310). Around 4–19 days per year show possible pollen events (PPE) when near-surface lidar observations of daily linear particle depolarization ratio >0.1 are coincident with high organic aerosol fraction. For PPE days with rainfall, aerosol size distribution observations show enhanced submicron particle concentrations consistent with pollen rupture events. For fungal spores, high fungal spore counts occur during late spring/early summer (DOY 110–195) and late summer/autumn (DOY 220–340). Based on size distribution observations, up to 7% of days have possible fungal spore rupture events (PFE) with higher aerosol number count specifically over the range expected for fungal spore fragment mobility diameter (20–50 nm). These short-lived PFE correlate with rainfall or occur after prolonged exposure to rainfall (e.g., >10 h). While the SGP site lacks direct measurements of bioaerosol and large particle sizes, this analysis suggests that PBAP primary emissions and rupture events could occur about 32 days per year, representing an important component of the aerosol budget during seasonal emissions.

Plain Language Summary Primary biological aerosol particles (PBAP) are emitted directly from the Earth's surface and can include pollen, fungal spores, and bacteria. They can act as nuclei for water droplets or ice crystals and are known to impact clouds and precipitation, and may influence both the regional and the global climate and hydrological cycle. Because measurements of many PBAPs are sparse, we use a suite of atmospheric data from the ambient aerosol and meteorological measurements from the Department of Energy's Atmospheric Radiation Measurements at United States Southern Great Plains site to indirectly identify possible emissions of pollen and fungal spores from the land surface. We estimate that PBAP can contribute to the local aerosol burden, especially during their peak emission periods.

1. Introduction

Primary biological aerosol particles (PBAP) are defined as solid airborne particles derived from biological organisms. Atmospheric aerosols are typically in the size range of ~1 nm–100 μm (Hinds, 1999; Seinfeld & Pandis, 2006), and PBAP have a typical size range of several nanometers to a few hundred micrometers (Cox & Wathes, 1995; Hinds, 1999; Jaenicke, 2005; Pöschl, 2005). PBAP can include viruses (particle diameters of ~0.1 μm), bacteria (~1 μm), fungal spores (~1–10 μm), pollen (20–100 μm), and other plant debris. PBAP can have a significant impact on atmospheric processes (Andreae & Crutzen, 1997; Després et al., 2012; Fröhlich-Nowoisky et al., 2016; Jaenicke, 2005; Lawler et al., 2020; Sofiev et al., 2006), including influencing clouds and precipitation by acting as nuclei for water droplets or ice crystals (Prenni et al., 2013; Schnell & Vali, 1975; Steiner et al., 2015), and may influence both the regional and the global climate and hydrological cycle (e.g., Andreae & Rosenfeld, 2008; Joung et al., 2017; Pöschl et al., 2010; Wozniak & Steiner, 2017; Zhang et al., 2014). Despite their possible importance, little is known about PBAP emissions as they are

Validation: Tamanna Subba, Allison L. Steiner
Visualization: Tamanna Subba, Allison L. Steiner
Writing – original draft: Tamanna Subba
Writing – review & editing: Tamanna Subba, Michael J. Lawler, Allison L. Steiner

challenging to estimate from existing atmospheric observations. Here, we focus on using a suite of observational data to estimate emission events of two types of PBAP from the land surface: pollen and fungal spores.

The life cycle of PBAP includes emission, transport, cloud processing, and eventual deposition (Figure 1). Pollen is the reproductive units of plants and contains the mail gamete used for reproduction in higher plants and grasses. The larger size of pollen (e.g., 20–100 μm) leads to high settling velocities and shorter atmospheric residence times, which drives a wide range in spatial and temporal variability. Pollen emissions are largely dependent on the vegetation species and plant functional type, and emissions have a strong seasonality depending on their flowering time (Wozniak & Steiner, 2017). Atmospheric concentrations of pollen are largely driven by anemophilous plants (i.e., those with wind-driven pollination strategies; Jones & Harrison, 2004; Lewis et al., 1983; Straka, 1975), with emissions and dispersion dependent on meteorological (e.g., temperature, wind, humidity and precipitation, and friction velocity) and climatological (e.g., temperature, soil moisture) conditions, as well as the physical characteristics of pollen such as shape, density, and viability (Després et al., 2012; Helbig et al., 2004; Veriankaitė et al., 2010). In addition, pollen emissions, transport, and atmospheric concentrations are also influenced by changes in land use patterns, anthropogenic activities, urbanization, weather events, and overall climate change (IPCC, 2007; Sofiev et al., 2006; Zhang et al., 2014; Ziska, 2016).

Surface temperature and humidity can influence pollen transport, with cooler and moister conditions limiting transport (Jones & Harrison, 2004). High temperature promotes pollen grain dispersal by inducing atmospheric instability (Kuparinen et al., 2009), and transfers them to higher altitudes while making them available for pollen-cloud interactions by acting as cloud condensation nuclei (CCN) and ice nucleating particles (INP) (Després et al., 2012; Diehl et al., 2001; Hader et al., 2014; Huffman et al., 2013; Pummer et al., 2012; Steiner et al., 2015; Vali et al., 2015; Wozniak & Steiner, 2017; Wozniak et al., 2018; Wright et al., 2008). Long-distance dispersal is possible via mechanical and thermal-induced updraft turbulent eddies (Kuparinen, 2006; Mahura et al., 2007) and is important in terms of plant ecology and evolution of plant species (IPCC, 2007; Kuparinen et al., 2009; Nathan et al., 2011; Tackenberg et al., 2003). Like other aerosol particles, PBAP are eventually removed from the atmosphere via dry or wet deposition.

Fungal spores are smaller than pollen (1–10 μm), with size varying with biological activity at the Earth's surface, age, meteorology, physico-chemical atmospheric processes (Després et al., 2007, 2012; Graham, 2003; Pöschl et al., 2010; Zhang et al., 2010). They are released from the terrestrial biosphere by changes in osmotic pressure and surface tension (Ingold, 1999; Lacey, 1996; Pringle et al., 2005). Depending on the stage of fungal spores during emissions (e.g., during the sexual, asexual, or both stages), spores contain specific sugars such as arabitol, mannitol, and sterol-like ergosterol compounds (Bauer et al., 2008; Lau et al., 2006), and hydrophobic compounds (Iannone et al., 2011). Prior studies have shown that fungal spores may account for ∼10% of organic carbon and ∼5% of PM_{10} at urban/suburban locations (Bauer, Kassper-Giebl, Loflund, et al., 2002, Bauer, Kasper-Giebl, Zibuschka, 2002, Bauer et al., 2008) to ∼45% of PM10 in pristine tropical rainforests (Zhang et al., 2010), depending on the ambient conditions.

In addition to the primary emissions and transport, PBAP can undergo transformations in the atmosphere that affect their size and number, and both pollen and fungal spores have been observed to rupture under atmospheric conditions. Under high humidity, large sized pollen grains can rupture, forming small fragments ranging from 30 nm to 5 μm (Miguel et al., 2006; Taylor et al., 2004). While rainfall can reduce pollen counts via wet deposition (Hughes et al., 2020), moist conditions can also induce pollen rupture processes (Rathnayake et al., 2017). Rupturing of pollen grains can be induced by buildup of the osmotic pressure in the grains (Taylor & Jonsson, 2004), and has been observed in the laboratory to occur under humid conditions (Grote et al., 2001, 2003; Taylor et al., 2004). In the ambient atmosphere, pollen rupture has been postulated to occur during thunderstorms, when vertical updrafts carry pollen grains to a cloud base where the high humidity condition ruptures them (Hughes et al., 2020) and subsequent downdrafts resuspend the respirable pollen fragments near the Earth's surface triggering acute allergic reactions (D'Amato et al., 2016; Taylor et al., 2002). Similarly, China et al. (2016) identified that osmotically induced fungal spores bursting episodes could result in the sporadic nanoparticle appearance events in the Amazon during the rainy season. This has also been observed at the United States Southern Great Plains site by Lawler et al. (2020).

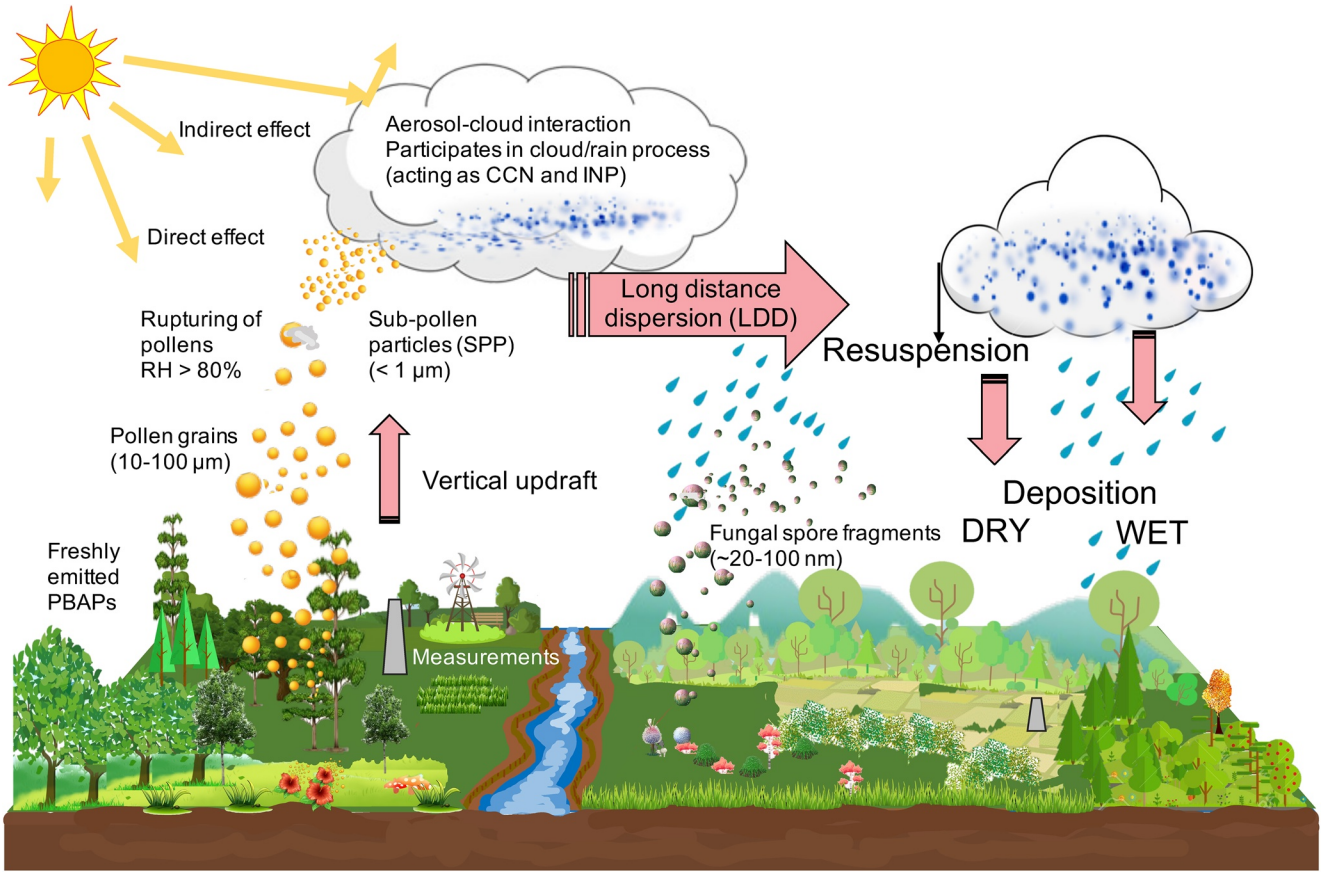

Figure 1. Schematic representation of the life cycle of primary biological aerosol particles (PBAP) (including pollen and fungal spores) in the atmosphere.

PBAP can act as CCN or as INP, thereby affecting clouds and precipitation. Fungal spores are a good candidate for CCN due to their smaller size, and the growth factor (GF) of fungal spores has been observed to be ~1.65 at 98% relative humidity (Lee et al., 2002), unlike pollen which show little or no growth in its geometric size. However, pollen can take up water up to three times their dry weight (Diehl et al., 2001), which is an important characteristic for CCN. The large sized pollen grains can behave as CCN at lower supersaturations, and even in very low concentrations these "giant CCN" quickly grow to large cloud droplet sizes resulting to rain formation (Möhler et al., 2007; Pope, 2010). A more likely contributor to CCN from pollen may be from ruptured grains. Depending on the amount of subpollen particles (SPP) generated from pollen rupture, the effects of SPP on clouds and precipitation can vary dramatically. Using ensemble simulations of the pollen rupture effect, Wozniak et al. (2018) found that low SPP generation rates (e.g., 10^3 SPP per grain) do not influence springtime precipitation. However, in the spring pollen season, if SPP were generated at high rates (e.g., 10^6 SPP per grain), the subsequent droplet growth and precipitation would be limited by the availability of water vapor, suppressing regional precipitation by up to 40%. Diehl et al. (2001) showed that pollen is capable of taking up a significant amount of water via the capillary effect during humid conditions and further found it to act as INP at relatively warmer temperatures (−12 to −18°C). Gute and Abbatt (2018) found that that pollen carries water-extractable compounds with IN activity and that the in-cloud oxidation may lower the IN ability of the pollens. And, at warmer temperatures, primary ice nucleation from biological particles can lead to secondary ice formation similar to that of the Hallet-Mossop process (Szyrmer & Zawadzki, 1997).

Despite their importance for both climate and health, little is known about the frequency and relevance of PBAP in the atmosphere as compared to other natural and anthropogenic aerosols. However, there is recent and growing interest in PBAP, including new monitoring techniques and the development of PBAP emissions and transport modeling frameworks to help advance the knowledge of regional and global PBAP

distributions (Després et al., 2012; Giesecke et al., 2010; Marceau et al., 2011; Spracklen & Heald, 2014; Wozniak & Steiner, 2017; Zhang et al., 2014). To understand the likelihood of occurrence of PBAP events, we utilize an existing data set with extensive aerosol measurements at the Department of Energy (DoE) Atmospheric Radiation Measurements (ARM) United States Southern Great Plains (SGP) site. While prior work has focused on natural and anthropogenic aerosols in the region, very little attention has been paid to other types of biological aerosols and their effect on clouds and precipitation. This work estimates possible pollen and fungal spore events from a suite of aerosol measurements at the ARM SGP site. We quantify the possible pollen and fungal spore emission event days by using the ambient aerosol measurement database along with the meteorological database from the DoE ARM measurements at SGP. This aims to provide an essential input to studies related to the climatic impact of PBAPs, climate-related changes in the airborne pollen and fungal spores, and human health.

2. Observations

2.1. ARM Measurements

Long-term (2011–2015) collocated measurements of aerosol physical, optical and chemical properties, and meteorological measurements are used from the United States Department of Energy Southern Great Plains (SGP) Atmospheric Radiation Measurement (ARM) site. Observations utilized from the Central facility (Lamont, OK) and the ARM user facility data archive (www.arm.gov) include:

1. Aerosol Chemical Speciation Monitor (ACSM) for aerosol composition;
2. Raman Lidar (RL) for vertical profiles of the aerosol extinction coefficient and linear depolarization ratio;
3. Merged particle size distributions (Marinescu et al., 2019)
4. Meteorological measurements including precipitation, and the temperature, humidity, wind, air temperature, and pressure sensors (THWAPS) system.

ACSM is a thermal vaporization, electron impact ionization mass spectrometer measuring bulk chemical composition. It provides data for nonrefractory submicron aerosol particles in real time at 30-min intervals, which are daily averaged when required. The ACSM samples aerosols ranging from 40 nm to 1 μm (Budisulistiorini et al., 2013; Ng et al., 2011), and mass concentrations for several chemical species can be derived from the ACSM data. We use mass concentrations of total organics, sulfate, nitrate, ammonium, and chloride in the present study.

ARM deploys a Raman Lidar, which is an optical remote sensing system designed to detect the real-time vertical distribution of clouds and atmospheric particles. We use the Raman Lidar vertical profiles (RLPROF) aerosol extinction coefficient and linear depolarization ratio profile, sampled at an interval of 10 min, which are averaged to the daily timescale in this analysis. Here, only data with a confidence score above 0.3 have been used, following the estimated random and systematic uncertainty values (e.g., Thorsen & Fu, 2015; Thorsen et al., 2015) provided in the same ARM data archive. One advantage to the depolarization ratio is that it can detect asymmetric particles (Burton et al., 2012). Prior studies have used linear depolarization ratios to estimate pollen emission events, where values >0.1 have been used an indicator of pollen (Noh et al., 2013; Sassen, 2008; Sicard et al., 2016). Sicard et al. (2016) found that high pollen counts at an urban site in Spain were well correlated with high volume and particle depolarization ratios, noting that values of 0.08 and 0.14 (with hourly maxima of 0.18 and 0.33, respectively) indicated the existence of the pollen plumes. It is possible that the depolarization could also be used to detect irregularly shaped fungal spores, but this technique has not been shown to accurately detect events, and therefore we use it for primary pollen emissions only.

Another existing measurement useful for the detection of possible biological particle events is the aerosol size distribution. We utilize the merged data sets developed by Marinescu et al. (2019) for 2011–2013, and specifically the merged product "CSA" which contains total aerosol number size distribution from a TSI 3010 condensation particle counter (CPC) along with the aerodynamic particle sizer (APS) and the scanning mobility particle sizer (SMPS), part of the tandem differential mobility analyzer (TDMA) system. Together, this data set covers the size range between ~7 nm and ~14 μm with 222 bins. We note that many primary biological particles, especially pollen and some fungal spores are too large to be captured in this data set.

2.2. Ancillary Data Sets

Daily pollen and fungal spore count data from the National Allergy Bureau (NAB) network from the American Academy of Allergy Asthma and Immunology (AAAAI) are obtained from the closest available stations to the SGP ARM DoE site. Two sampling stations in Oklahoma City, OK (35.5°N, 97.5°E) and Tulsa, OK (36.1°N, 96.0°E) are ~140 and 180 km to the south and southeast from the SGP DoE site, respectively. Pollen counts are collected with a Burkard volumetric air sampler or a Rotorod rotation impaction sampler. Data are reported as daily pollen/fungal spore concentrations (grains m^{-3}), which is the number of grains/spores per volume of the air sampled over 24 h. Pollen are grouped into 43 pollen categories with 38 specific genera and families for trees, grasses, and other herbaceous plants and four composite categories (Other Tree Pollen, Other Weed Pollen, Other Grass Pollen, and Unestimated Pollen). The total spore counts are divided into 23 different types of fungal spore species. Here, we use the total pollen and total spore counts to understand the likelihood of the PBAP events at SGP.

The Interagency Monitoring of Protected Visual Environments (IMPROVE) data are also used to understand regional aerosol chemical composition (Hand et al., 2012). The network collects 24 h aerosol samples every 3 days for gravimetric and composition analysis. IMPROVE fine dust/soil data from four sites near the SGP for the period 2002–2016 were considered to be representative for regional scale dust events around the SGP site. This mass of the fine dust aerosol is calculated assuming normal oxides of typically occurring soil species (Dust = 2.20 × Al + 1.63 × Ca + 2.42 × Fe + 2.49 × Si + 1.94 × Ti), including aluminum (Al), calcium (Ca), iron (Fe), silicon (Si), and titanium (Ti) (Hand et al., 2012; Malm et al., 1994). These data sets are used to distinguish dust particles from our estimations of possible PBAP particles.

The Cloud-Aerosol Lidar and Infrared Pathfinder Satellite Observation (CALIPSO) satellite (Omar et al., 2009; Winker et al., 2007) provides vertical aerosol and cloud data from June 2006. CALIPSO carries the Cloud-Aerosol Lidar with Orthogonal Polarization (CALIOP) instrument, which can measure the vertical structure of the atmosphere at three channels, and its repeat cycle is 16 days (Winker et al., 2007). The CALIOP aerosols or clouds classification feature have been validated in earlier studies (Bhoi et al., 2009; Kim et al., 2008; Liu et al., 2009; Omar et al., 2009). CALIPSO classifies several aerosol subtypes, including: (a) clean marine, (b) dust, (c) polluted continental, (d) clean continental, (e) polluted dust, (f) smoke, and (N/A) not applicable/not identifiable aerosol types. N/A, clean continental, and polluted continental subtype have a possible chance of including PBAP aerosols. Here, in order to distinguish days with high soil dust emission (Omar et al., 2009) CALIPSO, vertical profiles of aerosol subtypes, depolarization ratio, and total aerosol extinction from 2011 to 2015 are used (https://asdc.larc.nasa.gov/project/CALIPSO).

2.3. Methodology

The long-term aerosol and meteorological measurements at the SGP site are used to estimate possible PBAP days having either pollen and/or fungal spore events. First, the measured AAAAI pollen/fungal spore counts are evaluated during 2003–2010 (based on data availability) to define climatological time periods of maximum pollen and fungal spore emissions. Although these pollen counts are not colocated with the ARM data, they provide a climatology of peak PBAP emission periods, which can then be used with ARM aerosol and meteorological data to estimate possible PBAP event days.

Second, we assess the suite of aerosol measurements for the possible classification of primary PBAP events. These measurements include (a) ground-based lidar with depolarization to segregate days with near-surface linear depolarization ratios >0.1, which have been used in prior studies to identify asymmetric biological particles (e.g., Sicard et al., 2016) and (b) ACSM chemical composition to determine the dominant surface aerosol composition during the days identified by the AAAAI data. In general, PBAP contains primarily organics, whereas anthropogenic-influenced aerosol events will have significant fractions of inorganic species such as sulfates and nitrates. Therefore, days having organics as one of the major constituents of the aerosols were further segregated. Taken together, these days were designated as possible primary pollen emission days. Due to the lack of sufficient information, the estimation of the primary fungal spores has not been included here.

Third, the TDMA database was analyzed to determine possible PBAP rupture events. Using detailed chemical composition data, Lawler et al. (2020) found that fungal spore rupture events could be estimated in

the 20–50-nm size range. The compounds estimated during the suggested rupture events include C_6 sugar alcohols and pyrolysis products of chitin, which is specifically found in the cell walls of fungi. They also observed that these nanoparticle events are sometimes accompanied by depletion of larger (70–300 nm) sized particles. In that study, only events with low aerosol sulfate mass fractions were considered to avoid the influence of concomitant new particle formation. Lawler et al. (2020) noted that the fungal spore events occurred over a brief period of time, sometimes appearing only for minutes. These events did not significantly show particles of size range smaller than 15 nm, which would be likely in the case of new particle formation and were therefore attributed to fungal spore rupture events. Previous studies have demonstrated that the new particle formation events at SGP is characterized by increase in sub-15-nm particles (Chen et al., 2018; Hodshire et al., 2016; Nieminen et al., 2018). The SGP fungal nanoparticles are consistent with the suspected fungal nanoparticle bursts in the Amazon, which were also unaccompanied by larger particles (up to 500 nm) (China et al., 2016). A previous study by Wang et al. (2016) at the ARM site found that airborne soil organic particles which are directly injected into the atmosphere by rain impaction have a much larger characteristic size (about 0.5 μm). Also, in the case where rain impaction at the surface directly injects fungal nanoparticles into the atmosphere, it is expected that there would be wide range of particle sizes. Hence, the emissions considered during these types of events are thought to be dominantly driven by fungal spore germination and/or chemically or osmotically induced bursting (Bartnicki-Garcia & Lippman, 1972; Lawler et al., 2020; Wang et al., 2016).

We estimate possible fungal spore rupture events as days with (a) a peak of particles in the 20–50-nm size range, (b) a depletion of larger (70–300 nm) and smaller (<15 nm) particles, (c) following rain events, and (d) with an abundance of the organics from the ACSM observations. Similarly, pollen rupture events are estimated as the days having higher particle number concentrations within 1 μm during possible pollen event days and periods of rainfall.

3. Results and Discussion

3.1. AAAAI Pollen and Fungal Spore Counts

Because counts of pollen and fungal spores are not observed at most atmospheric observation sites, we use the closest available AAAAI measured counts to the SGP ARM site. The long-term (2003–2010) averaged daily total pollen count measured at two sites in Oklahoma City (OKC1 and OKC2) and Tulsa (TL1 and TL2) indicate two distinct time periods with high total pollen counts, with the first occurring in the late winter/early spring (DOY 50–120) and the second occurring in the late summer (DOY 240–310) (Figure 2). OKC1 showed a large increase in the pollen count in one of the winters (2004), leading to higher pollen counts in December and January at this site. The annual averaged pollen count is 165/126 grains m^{-3} for OKC1/OKC2 and 300/192 grains m^{-3} for TL1/TL2 respectively. Over the time period of available data, the maximum daily averaged total pollen counts during 2003–2010 ranges from 1,577 to 14,476, 1,083 to 4,769, 2,879 to 27,977, and 2,699 to 7,350 grains m^{-3} at OKC1, OKC2, TL1, and TL2 sites, respectively, indicating the strong day-to-day variability of the primary emissions. Prior analysis by Wozniak and Steiner (2017) determined that the first peak in the spring is driven by *Juniperus* and deciduous trees, with the second peak in the fall dominantly from *Ambrosia* (ragweed) (Howard & Levetin, 2014) and a late C_4 grass peak (Wozniak & Steiner, 2017).

At the four sites (OK1/OK2/TL1/TL2), the highest seasonal averaged total pollen count is observed in the spring (March-April-May, MAM) (295/255/826/514 grains m^{-3} by site), with a dominant contribution from *Cupressaceae*, *Morus*, and *Quercus*. During the winter (December-January-February; DJF), the average of the total pollen counts at OK1/OK2/TL1/TL2 sites is 175/65/123/58 grains m^{-3} with the maximum pollen count dominated by *Cupressaceae*, although we note that this may be influenced by long-distance transport (Howard & Levetin, 2014). In fall (September-October-November; SON), the average maximum count is dominated by *Ambrosia* with the average total pollen count at OK1/OK2/TL1/TL2 sites of 144/105/186/135 grains m^{-3}. Summer (June-July-August; JJA) pollen counts are relatively low, with total pollen of 36/33/49/41 grains m^{-3} at OK1/OK2/TL1/TL2 sites and predominantly from grasses (Graminacea/Poaceae). Overall, this temporal variation of pollen counts near the SGP site suggests that pollen emissions have a potential impact on the interannual/seasonal variation of the columnar aerosol loading, particularly in the spring when counts are the highest.

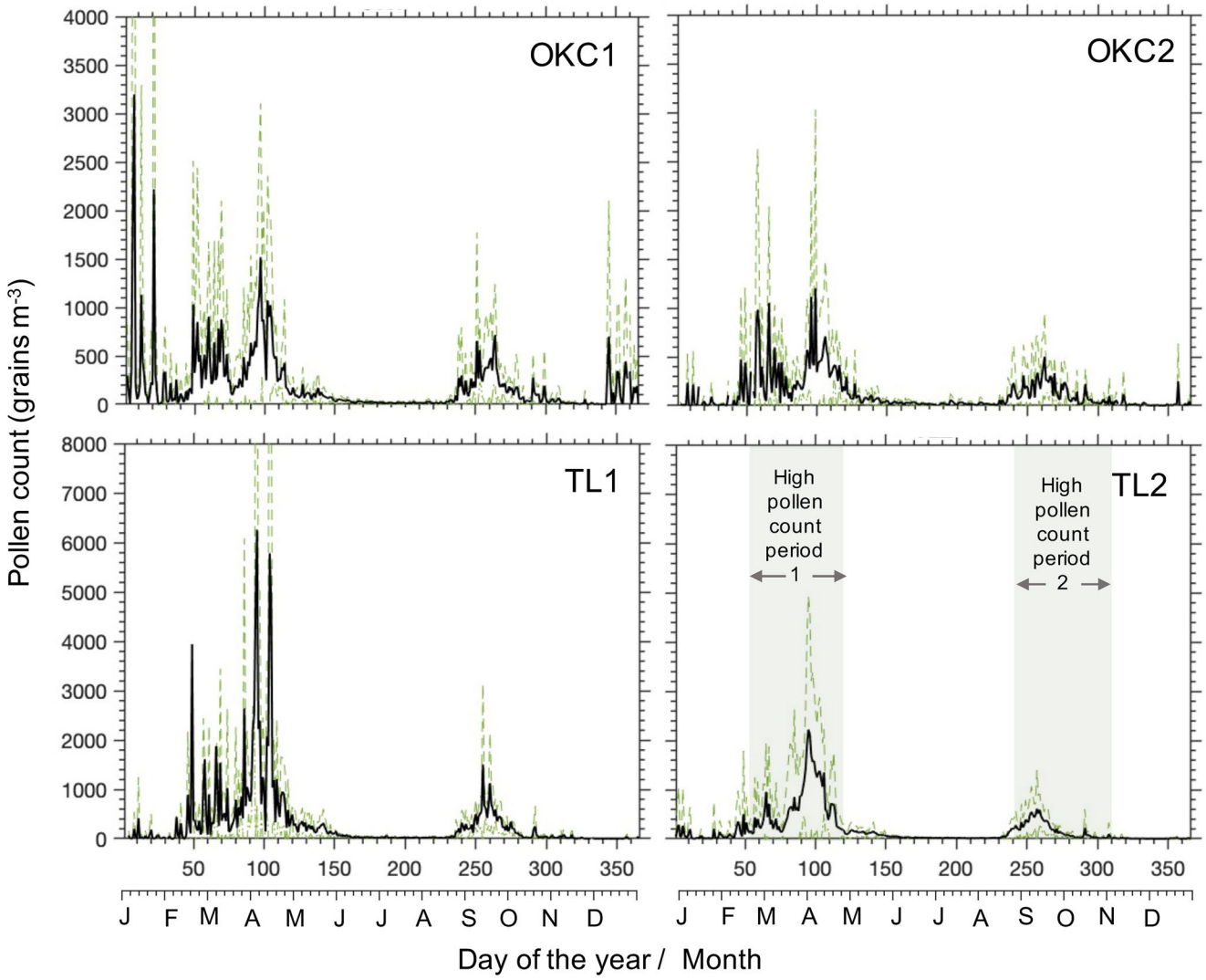

Figure 2. American Academy of Allergy Asthma and Immunology (AAAAI) total pollen counts for two Oklahoma City sites (OKC1 and OKC2) and Tulsa sites (TL1 and TL2). Black solid line represents the multiyear (2003–2010) average, green dashed and dotted lines indicate ±one standard deviation. Gray shaded region indicates the two pollen emission time periods (day of year [DOY] 50–120 in the spring and DOY 240–310 in the fall).

Averaged (2003–2008) daily total fungal counts measured at two Tulsa sites display two distinct time periods with high total fungal spore counts, with the first occurring in the late spring/early summer (DOY 110–195) and the second occurring in the late summer/autumn (DOY 220–340) (Figure 3). The annual averaged total fungal spore count is 6,515/6,022 spores m^{-3} for Tulsa sites 1 and 2, respectively. The highest number of fungal fragments belongs to *Cladosporium* (3,374/3,073 grains m^{-3} in site TL1/TL2) followed by undifferentiated *Ascospores* (2,222/1,359 grains m^{-3} in site TL1/TL2) in both the sites. Other species like undifferentiated *Basidiospores* (624 grains m^{-3} in site 2), *Stemphylium* (430 grains m^{-3} in site 1), *Diatrypaceae* (268 grains m^{-3} in TL1), *Smuts/Myxomycetes* (180/280 grains m^{-3} in site TL1/TL2), *Penicillium/Aspergillus* (203 grains m^{-3} in site TL2), and *Alternaria* (177/193 grains m^{-3} in site TL1/TL2) also shows considerable counts. Each fungal spore taxa shows a distinct seasonal behavior, e.g., *Cladosporium* spores highly influence both seasonal maxima whereas the undifferentiated *Ascospores* show just a single peak during first phase of fungal spore events. In subsequent analysis, we consider only the total fungal spore counts yet note that these seasonal differences might be useful for process-level emissions analysis.

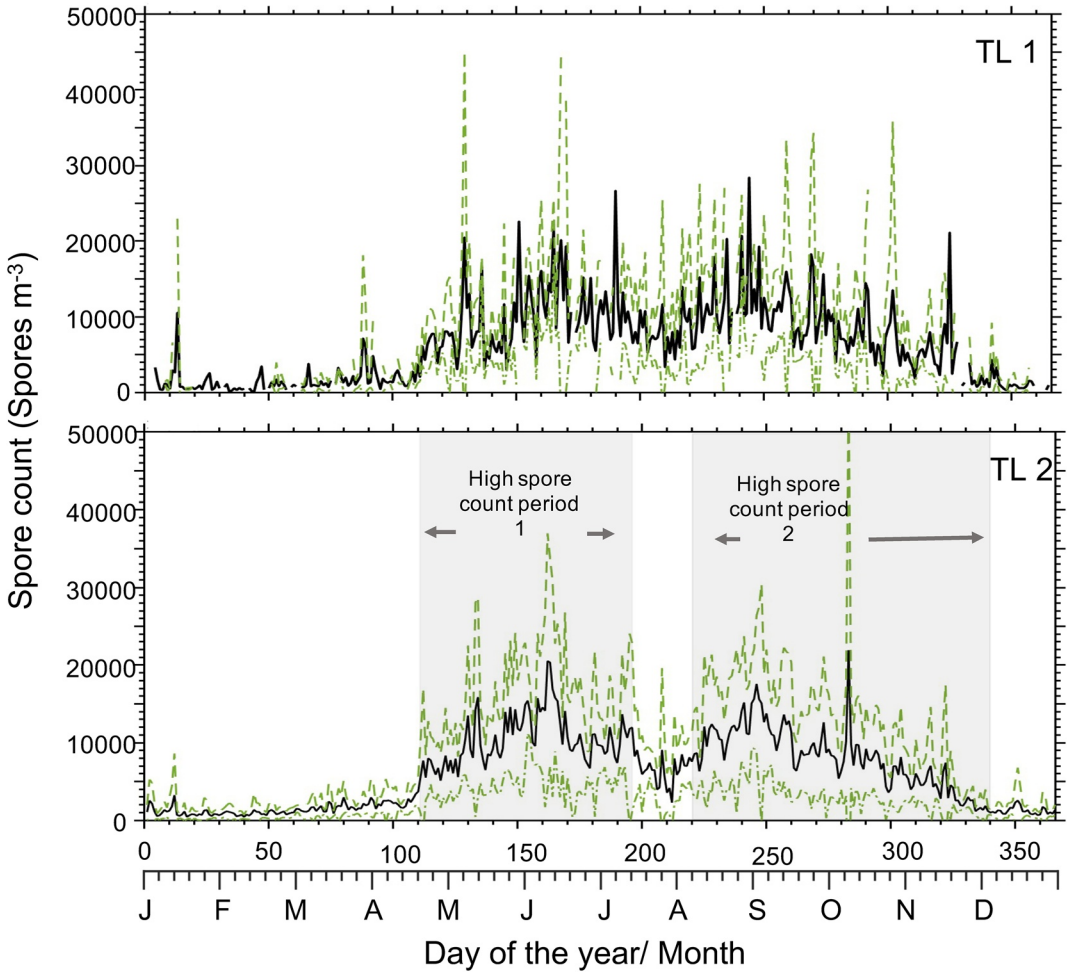

Figure 3. American Academy of Allergy Asthma and Immunology (AAAAI) total fungal spores counts for two Tulsa City sites (TL1 upper; TL2 lower). Black solid line represents the multiyear (2003–2008) average, green dashed and dotted lines indicate the ±one standard deviation. Gray vertical lines in the second panel indicate the two fungal spore emission time period (day of year [DOY] 110–195 in the late spring/early summer and DOY 220–340 in the late summer/autumn).

3.2. Bulk Aerosol Properties

3.2.1. Lidar Vertical Profiles

The real-time vertical distribution of atmospheric aerosol particles is evaluated using aerosol extinction coefficients from RLPROFs available from 2011 to 2015 at the SGP site. Aerosols are present predominantly below 1.5 km, with higher values of the extinction coefficient near the surface (<0.5 km) indicating aerosol emission sources at or close to the surface (Figure 4). The average annual aerosol optical depth (AOD) from RLPROFs during 2011–2015 was 0.03 within 1.5 km, with significant variation in the interannual seasonal aerosol loading. The highest climatological AOD was during winter (0.035 within 0.5 km and 0.052 from 0.5 to 1.5 km). This was followed by autumn/spring with values 0.023/0.022 below 0.5 km and 0.037/0.039 within 0.5–1.5 km and summer with values ~0.01 within 1.5 km. Overall, these low AOD values suggests relatively low near-surface aerosol concentrations at the site. However, we see number of short-lived aerosol events with AOD values much higher than that of the background mean. Frequently in all years during the winter, the early spring and the autumn months, daily AOD values can exceed 0.3 (Figure 4). These higher AOD events are likely associated with the local anthropogenic emissions such as agricultural, vehicular, industrial, and the local burning activities, and the natural emissions such as dust, natural biomass burning and PBAP, and augmented by the long-range transport of aerosols.

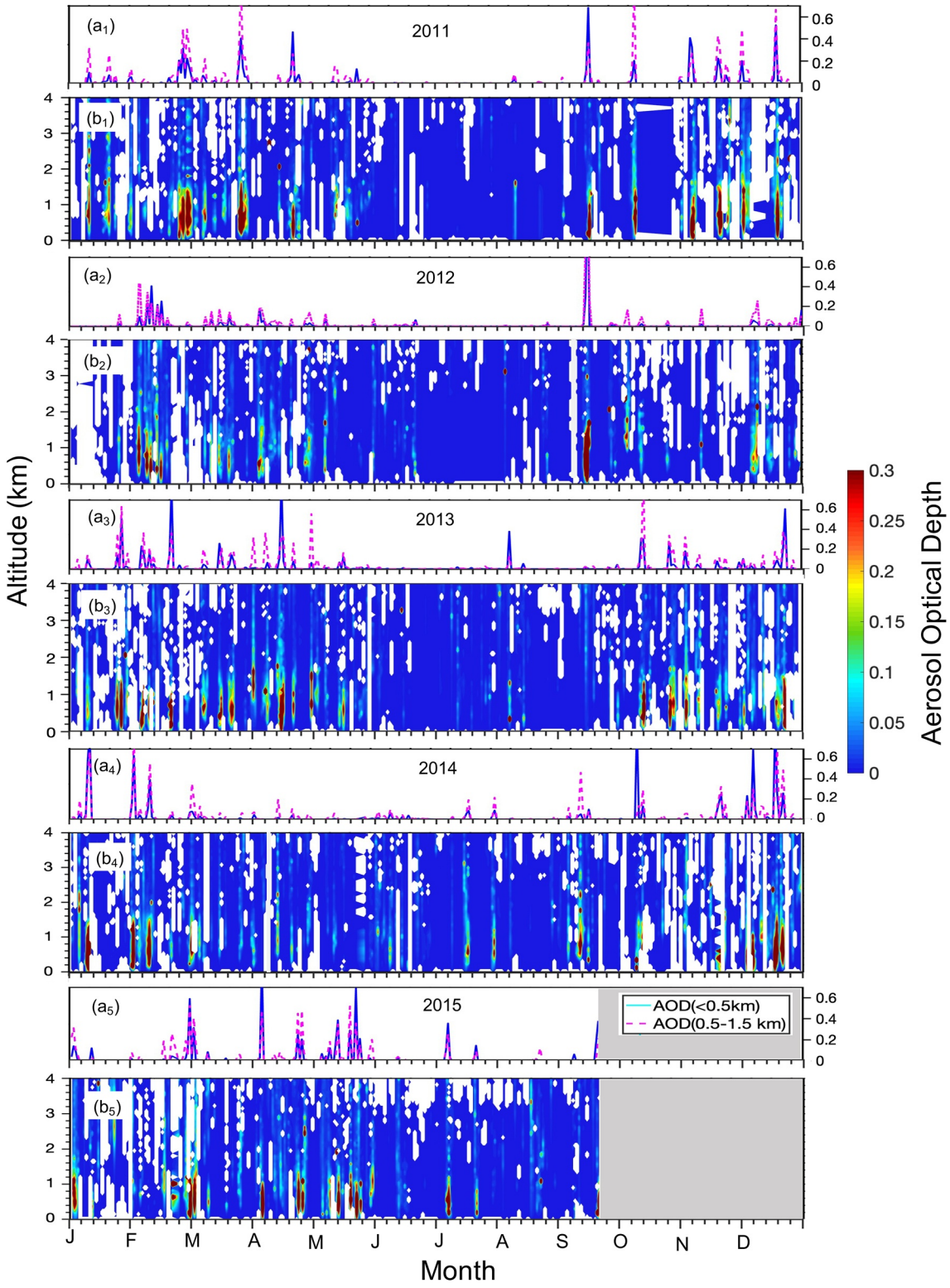

Figure 4. Daily aerosol optical depth at Southern Great Plains (SGP) Atmospheric Radiation Measurements (ARM) site in the first 1.5 km (pink) and 0.5 km (blue) from the Raman Lidar for 2011 to 2015 (a1–a5). Contours represent the daily vertical profiles of the aerosol extinction coefficients for respective years (b1–b5). Gray shading represents missing data.

Aerosols above the atmospheric boundary layer (ABL) do occur episodically and are likely associated with long-range and convective transport processes (Bourgeois et al., 2015; Lee et al., 2019). The variation in the vertical loading of the aerosols indicates that aerosol loading over SGP can be influenced by the distant sources apart from those on the ground. Based on HYSPLIT back trajectories, Parworth et al. (2015) reported that the site was influenced by trajectories from both south and north during the spring transition, depending on high-pressure and low-pressure systems.

We also examine the Lidar linear depolarization ratio, as this can estimate the presence of asymmetric particles such as pollen, fungal spores, or dust. Higher depolarization ratios near the surface can provide evidence for emissions of PBAP, and prior studies have noted that high depolarization ratios near the surface and extending into the boundary layer over time can be a signature of pollen emission events (e.g., Sicard et al., 2016). We use near-surface depolarization values to estimate the possible pollen event days in Section 4.1.

Comparing Figure 4 and Figure 5, there are many instances where a high near-surface extinction coefficient is not coupled with higher near-surface depolarization ratios (e.g., spring 2011, winter 2014, and summer 2015), indicating the overall aerosol loading at a location is influenced by multiple sources. However, on days when there is a high near-surface extinction from aerosols as well as a high near-surface depolarization ratio, it suggests that PBAP may provide a substantial contribution to the overall aerosol extinction coefficient. Hence, the near-surface high aerosol optical depth and depolarization ratios can together represent the existence of PBAP.

3.2.2. Distinguishing PBAP From Dust

Typically, high depolarization ratios are attributed to dust, yet they could also be driven by the presence of PBAP. A wide range of dust depolarization ratios has been reported from prior short-term and long-term experiments. Dust aerosols are classified by satellite-based algorithms (CALIPSO) with the volume depolarization ratio >0.075 (Mielonen et al., 2009; Omar et al., 2009) and the linear particle depolarization ratio at 532 nm to be ∼0.22 (He & Yi, 2015) to 0.25–0.35 from ground-based measurements from Barbados (Haarig et al., 2016) and Morocco (Freudenthaler et al., 2009). Similarly, a laboratory-measured linear depolarization ratio ranged from 0.03 to 0.3 at 488 and 552-nm wavelengths (Järvinen et al., 2016). Daily mean particle depolarization ratios at 532 nm of the pollen layers have been identified to be 0.38 ± 0.23 (Bohlmann et al., 2019), with a volume depolarization ratio of 0.08–0.14 (Noh et al., 2013; Sicard et al., 2016) and 0.30 (Sassen, 2008) on days with high pollen counts. Overall, the available studies suggest that the depolarization ratios of pollens are slightly higher than that of dust. However, it is difficult to clearly separate the two species solely on the basis of depolarization ratios without additional experimental evidence.

Because, we do not have sufficient observations to separate the coexistence of dust and pollen, we estimate the annual distribution of dust particles and exclude days with higher concentrations of dust. Dust composition is not included in the ACSM data; therefore, we use IMPROVE data from sites near the SGP available during the period 2002–2016 as representative for regional scale dust events that may influence surface concentrations at the SGP site. The archived IMPROVE data from nearby stations Cherokee Nation (∼290 km away in the east direction with 9 years of data), Stillwell (∼323 km away in the southeast direction with 7 years of data), Tallgrass (∼240 km away in the north direction with 15 years of data), and Wichita Mountains (∼290 km away in the southwest direction with 15 years of data) show a consistent seasonal cycle with the most prominent soil mass during summer and the highest concentrations during July (Figure 6). This peak emission period of soil is coincident with the lowest emission period of PBAP (170–230 days of the year). Very occasional dust peaks are observed during spring, and are the strongest at the Wichita Mountains site (Figure 6). To avoid the influence of the high soil emissions during the pollen event days, we consider the IMPROVE daily soil concentrations for each of the possible pollen event days (Section 4.1).

Another method to remove days with high soil dust emission is by using CALIPSO (Mielonen et al., 2009; Omar et al., 2009) vertical profiles. CALIPSO data sets were coincident for 14 PPE days during 2011–2015. Figure S1 shows two typical examples of CALIPSO profiles during PPE days. The first case on February 19, 2015 shows an example where the aerosols are unclassified (Omar et al., 2009), that is, a not applicable (N/A) aerosol type throughout the column of the atmosphere. However, the depolarization ratio is high from surface to 4 km, suggesting the presence of PBAP aerosols. The second case on April 09, 2013 shows

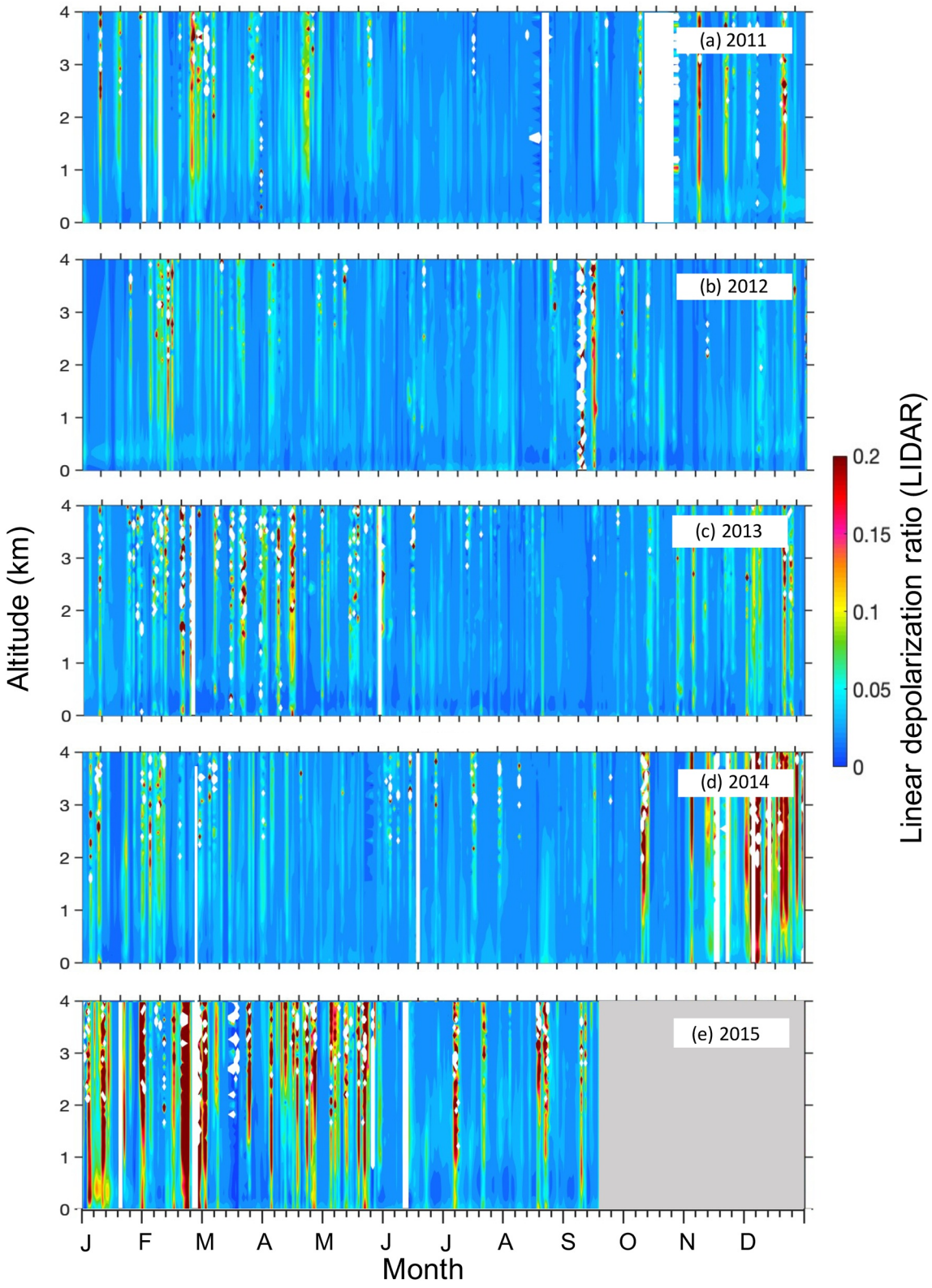

Figure 5. Daily profiles of linear particle depolarization ratio measured at Southern Great Plains (SGP) Atmospheric Radiation Measurements (ARM) site using Raman Lidar from 2011 to 2015 panels (a–e). Gray shading represents missing data.

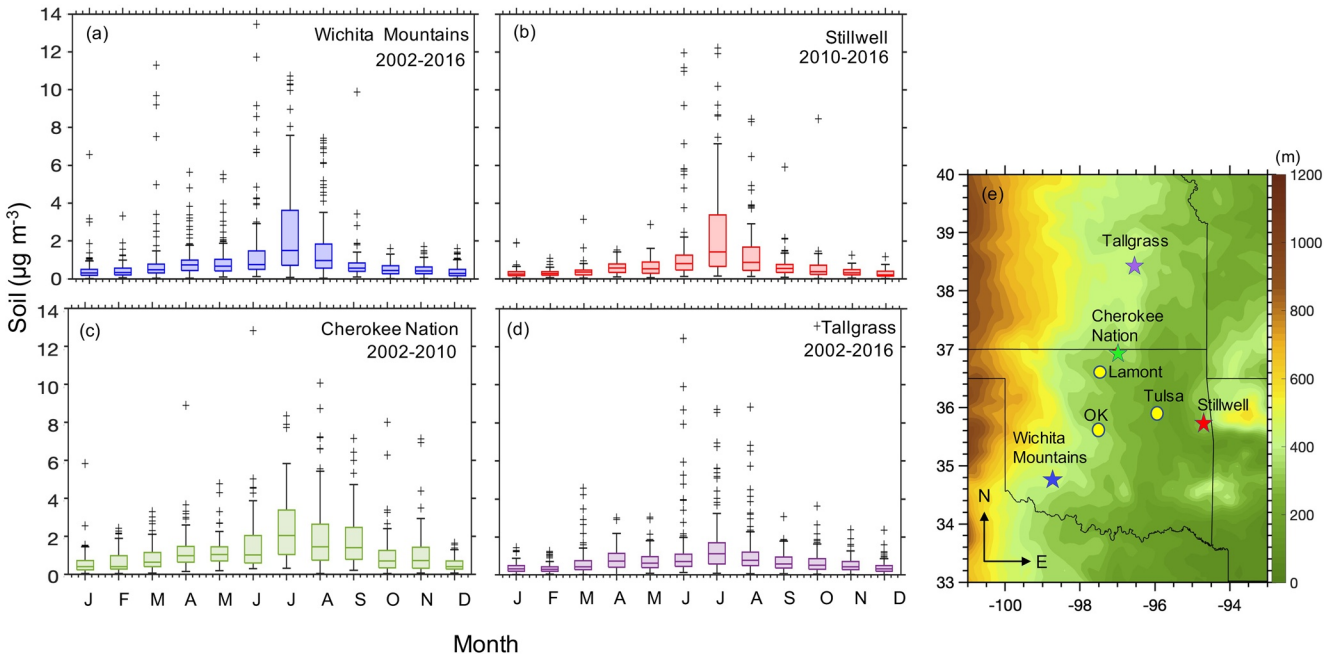

Figure 6. Box plot of annual soil concentrations obtained from Interagency Monitoring of Protected Visual Environments (IMPROVE) network at (a) Wichita Mountains (2002–2016), (b) Stillwell (2010–2016), (c) Cherokee Nation (2002–2010), and (d) Tallgrass (2002–2016) sites. (e) The site locations with altitude (m) color contours.

an example of unidentified aerosol types (N/A) closer to the ground (<1 km), with dust estimated aloft (>3 km), suggesting regional dust transport. However, the depolarization ratios near the surface are still high when the aerosol type is categorized as N/A type. Because we cannot clearly infer that the lower altitude particles are from PBAP, days having a profile similar to the April 09, 2013 case have been excluded from the total possible PPE count in Section 4.1.

3.2.3. ACSM Particle Composition Mass Concentration

Because meteorological conditions influence aerosol concentrations and emission processes, we evaluate temperature, relatively humidity, rainfall, and winds at the site (Figure 7). Generally, rainfall peaks at the site in the summer (3.2 ± 0.3 mm h^{-1}) with a minimum in the spring (1.0 ± 0.1 mm h^{-1}), yet there is substantial interannual variability during the data record. Year 2011 (annual average 0.3 ± 0.02 mm h^{-1}) and 2012 (annual average 0.2 ± 0.02 mm h^{-1}) were relatively dry years compared to 2013 (annual average 2.5 ± 0.2 mm h^{-1}), 2014 (annual average 6.0 ± 0.4 mm h^{-1}), and 2015 (annual average 2.0 ± 0.1 mm h^{-1}). 2012 was the driest year with very low annual hourly rainfall of 0.7 cm h^{-1} yr^{-1} compared to the wet years with heavy rainfall, such as 2013 and 2014 with annual hourly rainfall of 8.68 and 21.50 cm h^{-1} yr^{-1}, respectively. The site exhibits a continental climate, with average temperature highest in summer (26.7 ± 0.35°C) and lowest in winter (2.5 ± 0.31°C). The annual average relative humidity during 2011–2015 was 63.4 ± 0.37%, with seasonal variations reaching a maximum in winter (67.4 ± 0.66%) and a minimum in summer (58.4 ± 0.79%). Variable wind directions (Figure 7b) and their back trajectories (Figure S2) indicate that both nearby and distant possible aerosol sources and their precursors can be transferred to the SGP site.

ACSM measurements capture the submicron aerosol mass concentration at the SGP site from 2011 to 2015 (Figures 7 and 8). The total averaged particle mass concentration is 7.34 μg m^{-3}, with the highest value during summer (9.72 μg m^{-3}) and minimum value during autumn (4.8 μg m^{-3}). Total organics contribute the highest fraction of the total mass concentrations, with the annual averaged mass concentration of total organics of 4.01 μg m^{-3} (~54.63% of the total particle mass concentration 7.34 μg m^{-3}). This is followed by nitrate (16.08%, 1.18 μg m^{-3}), sulfate (~20.16%, 1.48 μg m^{-3}), ammonium (~8.72%, 0.64 μg m^{-3}), and chloride (~0.41%, 0.03 μg m^{-3}) (Figure 8). The mass concentration of SO_4^{2-} is highest (~25%, 2.46 μg m^{-3}) in summer and lowest (~13%, 1.0 μg m^{-3}) in winter, with NO_3^- concentrations highest (~37%, 2.79 μg m^{-3}) in

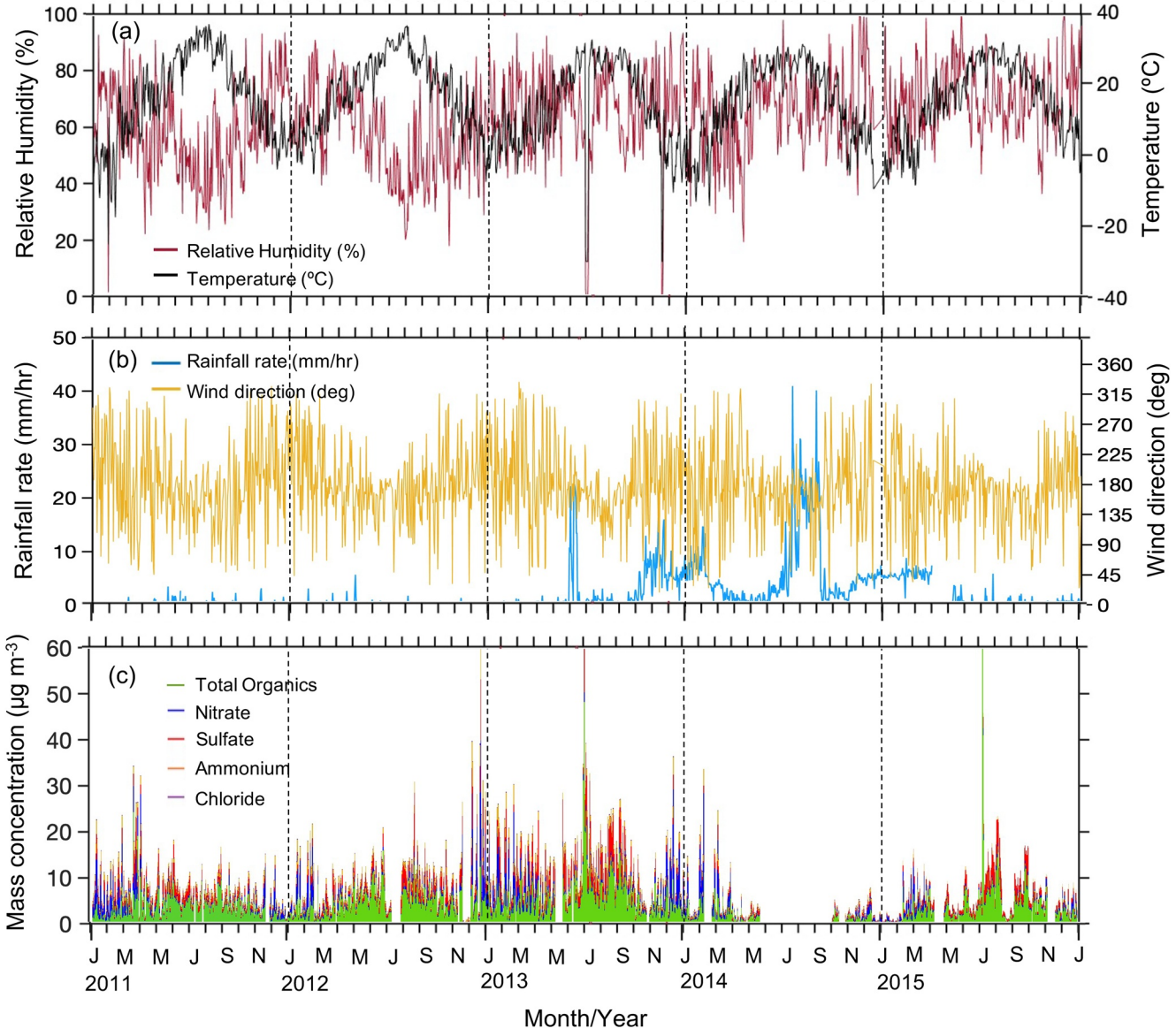

Figure 7. Meteorological and aerosol composition data at Southern Great Plains (SGP) Atmospheric Radiation Measurements (ARM) site using Aerosol Chemical Speciation Monitor (ACSM) from 2011 to 2015, including (a) Relative humidity (%) and temperature (°C), (b) Rainfall rate (mm h^{-1}) and wind direction (°), and (c) The daily aerosol composition concentration (μg m^{-3}) for total organics (green), nitrate (blue), sulfate (red), ammonium (orange), and chloride (purple). Dashed lines separate calendar years.

winter and lowest in summer (4%, 0.42 μg m^{-3}). Previous ACSM studies by Zhang et al. (2007) and Parworth et al. (2015) found the molar equivalent ratios of ammonium to anions (i.e., nitrate, sulfate, and chloride) to be nearly one, suggesting the particles are neutralized.

The annual mass concentration of each component is highly variable and exhibits substantial interannual variability, but it is possible to make some general conclusions about the seasonal cycle of aerosol composition. In a prior study analyzing aerosol composition at the SGP site from November 2010 to June 2012, Parworth et al. (2015) found that emissions of biomass burning organic aerosols and the formation of ammonium nitrate resulted in a high mass concentration of submicrometer during spring and winter months, respectively, with oxygenated organic aerosol and sulfate dominating in the summer season. During the 2011–2015 period, high values of nitrates (daily maxima of 10–20 μg m^{-3}) typically occur in winter due to lower PBL heights (Figure S3), lower temperature enhancement of the condensation of semivolatile species

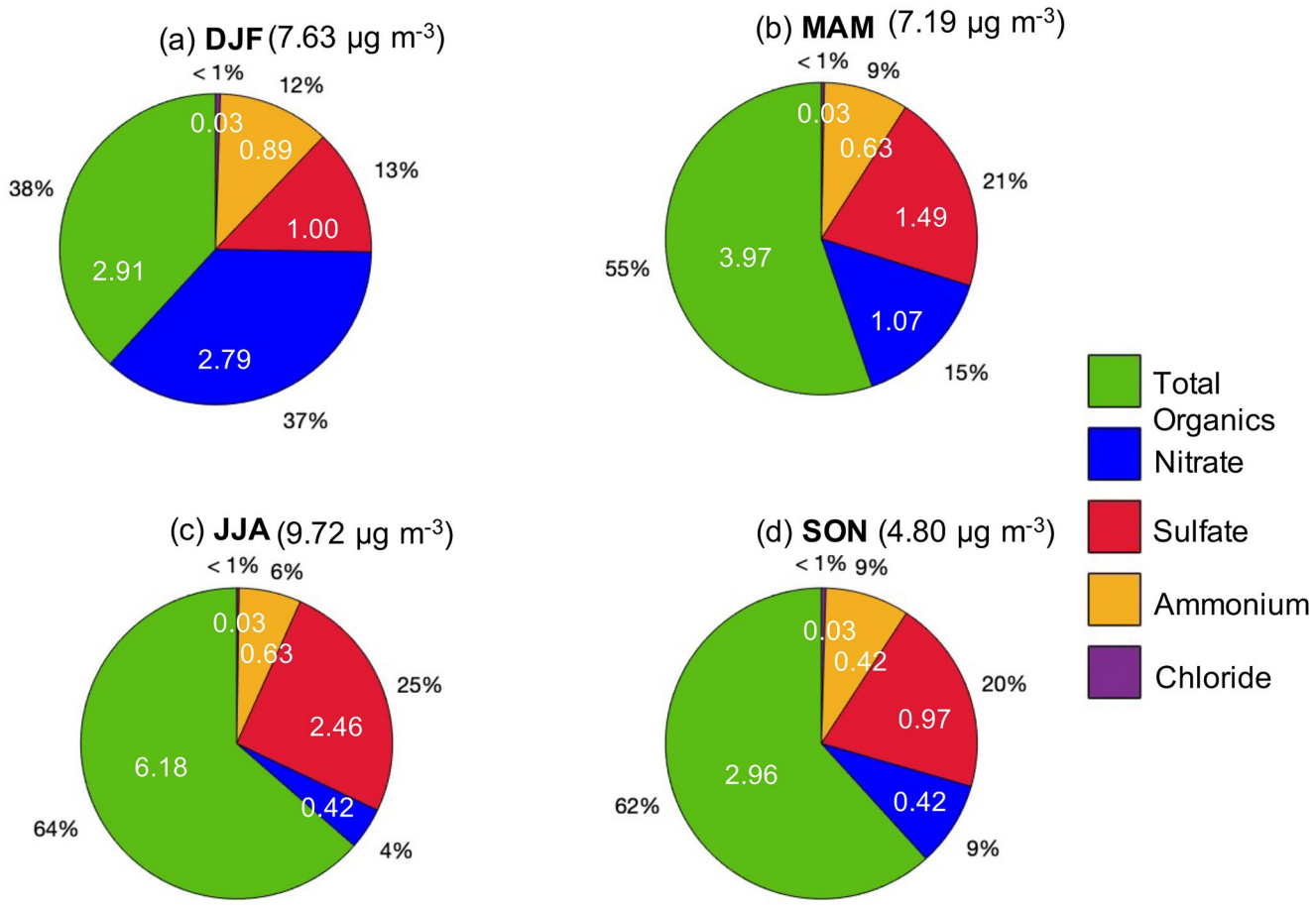

Figure 8. Seasonal submicron aerosol composition (2011–2015) (a) December-January-February (DJF)-winter, (b) March-April-May (MAM)-spring, (c) June-July-August (JJA)-summer, (d) September-October-November (SON)-autumn by mass (μg m^{-3}) and percentage. Colors represent aerosol composition for total organics (green), nitrate (blue), sulfate (red), ammonium (orange), chloride (purple).

such as NH_4NO_3, and local agricultural burning during winter and early spring (Lindley et al., 2019). The mass concentration of SO_4^{2-} peaks in summer, likely due to the sulfur dioxide emission sources around SGP as well as enhanced flow from urban areas to the southwest (Parworth et al., 2015).

To understand the influence of the various meteorological factors, we analyzed the aerosol composition with respect to meteorological parameters (Figure S4). Temperature showed distinct seasonal characteristics with higher NO_3^- and NH_4^+ during the colder months (DJF and MAM), with SO_4^{2-} and OC dominant during warmer months (JJA and SON). The dependence of aerosol composition with respect to the relative humidity was not present; however, the direction seems to play an important role in terms of aerosol loading over the SGP site, especially for OC and SO_4^{2-}. NH_4^+ showed a slight increase in loading with wind from the south in JJA and SON, and from the north during DJF and MAM. However, OC and SO_4^{2-} showed larger loading from the south during JJA and SON. However, variable wind directions at the SGP site suggest that other possible sources can also contribute to sulfate loading at the SGP site (Figures 7b and S4), and Parworth et al. (2015) noted higher SO_4^{2-} when winds were from the southwest. Anthropogenic emission sources are located southwest of the SGP site in southcentral Kansas and near Oklahoma City, and our analysis also found wind trajectories coming from these locations especially during February and March.

We hypothesize that PBAP emissions during late winter/early spring/early summer and autumn can influence the total organic composition of aerosols, hence making the organic fraction an important metric in estimating the PBAP events. In the aerosol compositional analysis, organic aerosols are high during late winter and early spring periods and dominate in JJA during 2011–2015. From the distribution of organics

with respect to wind direction (Figure S4), high magnitudes of organics are likely influenced by the winds from SE to SW directions during summer. Summer organic aerosol in the region is likely dominated by secondary organic formation from anthropogenic and biogenic precursors and local fire sources. Along with the existing studies (Melvin, 2018; NIFC, 2019; Parworth et al., 2015; Steiner et al., 2020), here, we have explored the MODIS fire radiative powers data (MCD14DL, collection 6, Giglio et al., 2016) for the period 2011–2015 (Figure S5). Both the medium (30–80%) and high (80–100%) confidence FRP data show high values during the summer months. More than 1 million ha area at Oklahoma including its neighboring states, Kansas, Texas, and Nebraska is highly affected by wildfire (Melvin, 2018; NIFC, 2019). Steiner et al. (2020) noted three significant grassland wildfires namely, the Anderson Creek, Starbuck, and Perryton wildfires in the Southern Great Plains during 2016–2017, and Donovan et al. (2017) found that the wild fire activity in Great Plain regions has been increasing in the past three decades. These events drive strong seasonal and interannual variability of aerosol loading over the SGP site when aided by the variation of the wind trajectories and other primary emission sources. Because our PBAP analysis focuses on the so-called "shoulder seasons" (late winter/early spring and the late summer/early autumn), biomass burning is relatively low during these time periods and we do not think that it would be the dominant contribution to organic aerosol.

3.2.4. Particle Size Distribution

In addition to composition, the particle size distribution can provide another indicator of possible PBAP emissions, despite its limited range to particles in the 20 nm–14-μm size range. The temporal distribution of the aerosol number concentration obtained using merged size distribution data at the SGP DoE ARM site during 2011–2013 (Marinescu et al., 2019) shows that most of the particles are smaller than 1 μm (Figure 9). Overall, 2013 was comparatively wetter than 2011 and 2012 (Figure 7), which may contribute to either greater biogenic source emissions from vegetation or more humid conditions that enable fine particle growth. This is also supported by higher aerosol loading in 2013 in the ACSM measurements, with an enhancement of the total organic particles during the high rainfall period (May-June; Figure 7c). Additionally, rainfall can enhance PBAP rupture rates, and it is possible that some of the increase in organic material may be from biological fragments from PBAP rupture or exposure to rainfall/high humidity conditions. In Section 4.2, we utilize these particle size distribution measurements to segregate the days having the size ranges from 20 to 50 nm, which is considered as a step toward the estimation of the possible fungal spore/pollen grain rupture event days.

From Figure 9, we have a comparatively low number of aerosols larger than 1 μm, with the corresponding volume size distribution showing slightly different features (Figure S6). The small volume of the <1 μm aerosols contributes to lower volume concentration despite being larger in number, with larger particles driving higher volume concentrations that are likely dominantly from PBAP or dust. Both 2012 and 2013 exhibits high volume concentrations during summer (150–220 DOY) and occasionally large volume concentrations during spring and fall (60–150 and 220–320 DOY). From the seasonal cycle of both PBAP (Figures 2 and 3) and dust concentrations (Figure 6), we infer that large values during summer can be related to the high values of soil/dust (Figure 6) whereas the occasional peaks during spring and fall are more likely related to the PBAP. Here, it is important to consider the large number of missing data points especially for 2011 and 2013; therefore, these data sets are not the exact or complete representation of the particle volume distributions.

4. PBAP Event Detection

4.1. Pollen Event and Pollen Rupture Detection

To consider impacts of all the possible local and distant emissions sources and the prevalent meteorological conditions, we combined several observations to estimate PPE days. The daily linear particle depolarization is analyzed to estimate possible primary pollen emission events. The volume depolarization ratio for primary pollen emissions has been estimated to range from 0.08 to 0.14 (Noh et al., 2013; Sicard et al., 2016) to 0.30 (Sassen, 2008), and we first select possible depolarization signal values with a linear particle depolarization ratio >0.1 near the surface where emissions could be detected.

Prior studies have shown that PBAP such as pollen consists of organic matter (Bozzetti et al., 2016; Després et al., 2012; Sun & Ariya, 2006; Zhu et al., 2015), and we utilize ACSM data to provide information about the

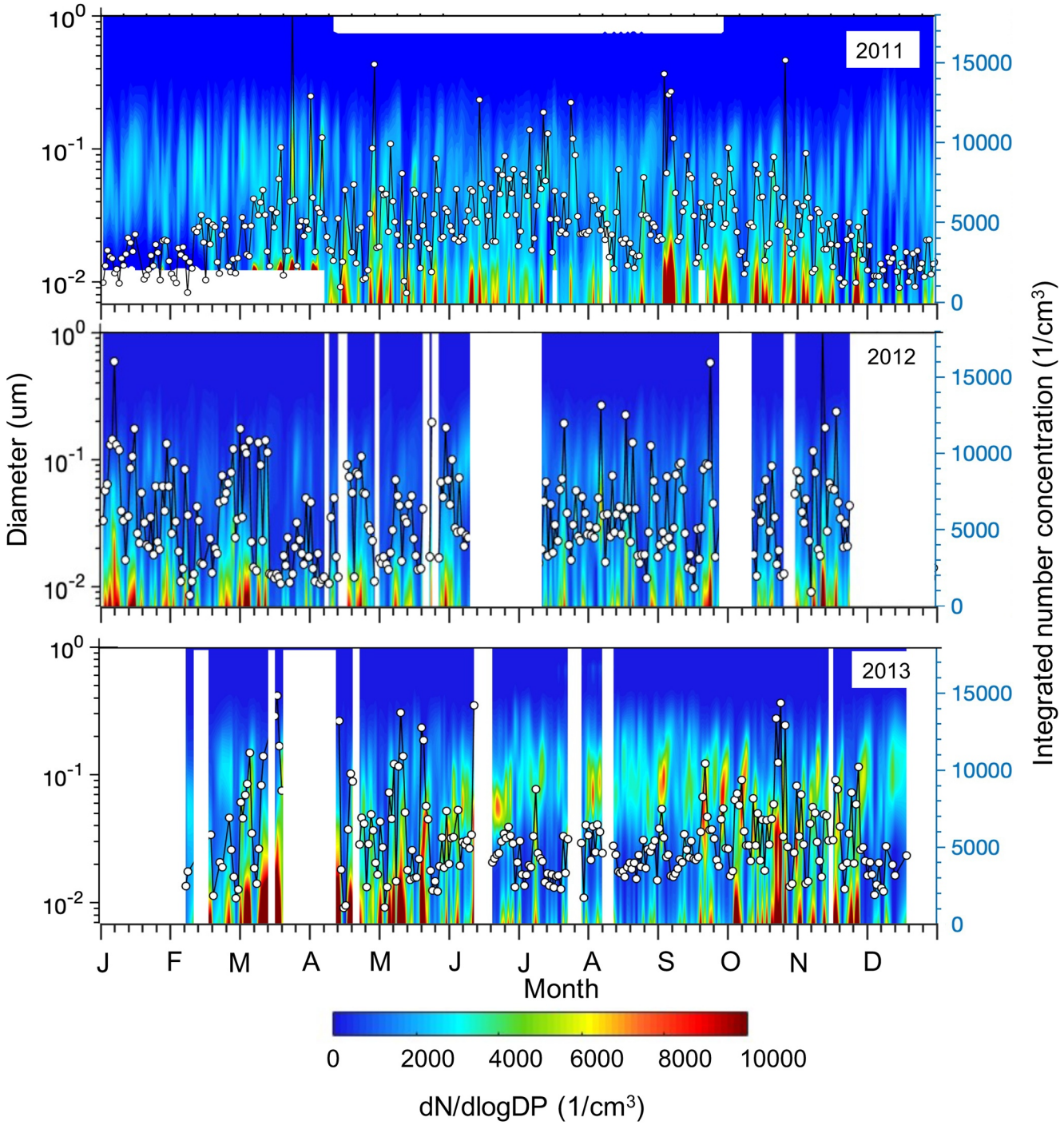

Figure 9. Time series of the aerosol number size distribution (dN/dlnDp, in color shading) for 2011–2013 as a function of diameter (left axis) using merged (CSA, CPC + SMPS + APS) data at Southern Great Plains (SGP) Atmospheric Radiation Measurements (ARM) site. White filled circles represent the total integrated number concentrations (right axis) data set used in this study.

composition during high depolarization days. The organic concentration from ACSM is primarily used to determine if there is a dominance of other aerosol species on that day, which would suggest advection to the site of all aerosol sources, and could the influence of number concentration on the total aerosol loading for that day. Also, ACSM sulfate data are used to exclude nucleation-sized particles and allow the detection of fragments of PBAP aerosols. Generally, organics provide the highest fraction of particle composition mass

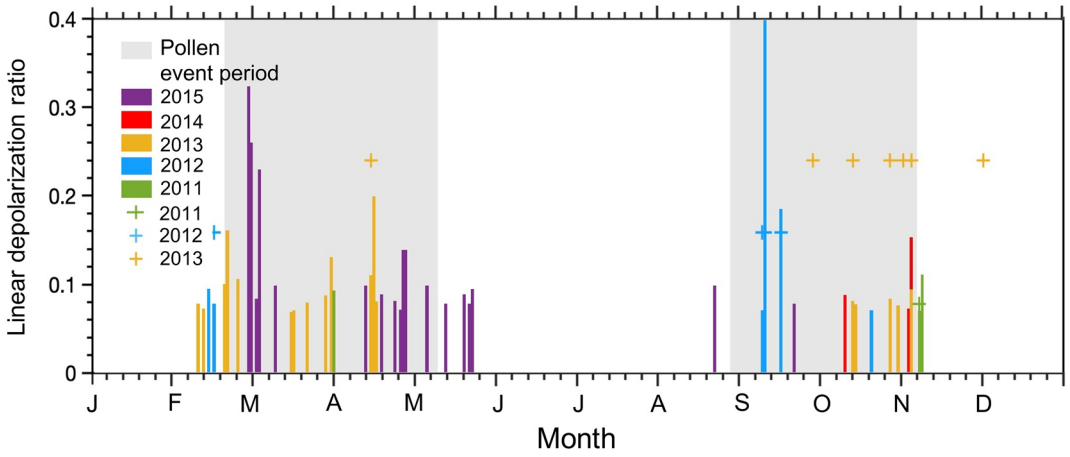

Figure 10. Annual distribution of days estimated as the possible primary pollen emission event (bars) and pollen rupture event (crosses) days by year of analysis. Colored bars and crosses show the averaged near-surface (<500 m amsl) linear depolarization ratio for each possible event. Gray shading indicates the pollen event periods estimated from nearby pollen count stations (Figure 2).

concentrations during pollination periods (48.76%, 3.45 μg m^{-3}) followed by nitrate (24.78%, 1.74 μg m^{-3}), sulfate (16.55%, 1.17 μg m^{-3}), ammonium (9.51%, 0.67 μg m^{-3}), and chloride (0.40%, 0.03 μg m^{-3}).

From the selected days with high depolarization ratios, we consider only those days with predominance of total organics as possible pollen event (PPE) days (Figure 10). Most of the PPE days fall during the two pollen event periods, which are late winter/early spring (DOY 50–120) and late summer (DOY 240–310). Further the merged product has been used to estimate the days having higher volume concentration during the pollen event period. As mentioned in Section 3.2.4, 2011 data sets are unavailable and there are very few days (4 days in 2012 and 5 days in 2013) coincident with the PPE days. IMPROVE observations at four different sites around SGP shows that the daily soil concentration during pollen event days was 0.32 μg m^{-3}. Two of the PPE days where the values of soil emission went above 1.0 μg m^{-3} (March 16, 2015 with 1.15 μg m^{-3} and October 13, 2015 with 1.09516 μg m^{-3}) have been excluded from the total possible pollen emission days to exclude possible confounding effects of dust.

Based on these two criteria, we estimate about 4–19 days per year during the total study period 2011–2015 as PPE days, or equivalent to an average of 12 days per year. To estimate possible pollen rupture events, we use the merged size distribution and the hourly rainfall measured in conjunction with the prior estimation of PPE based on the depolarization ratio >0.1 and a dominant composition of organics. Using the available data over the three-year period (2011–2013), we estimate a total of 2–6 days per year with possible pollen rupture events.

Figure 11 shows a typical example of a day (DOY 81, March 22, 2013) estimated as a PPE day. The vertical profiles with greater extinction near the surface suggest that the aerosol loading on this day was likely related to near-surface emissions. Specifically, near-surface high extinction coefficients (within the first 0.25 km) during 06:00–16:00 h (UTC) are high (>0.5), and the height of maximum extinction slowly increases in altitude at around 17:00 UTC, reaching the height of around 0.7 km at around 22:00 UTC (Figure 11a). The diurnal variation of linear particle depolarization ratio profile shows a similar pattern to the aerosol extinction coefficient, with greater depolarization values (>0.1) close to the surface, which slowly starts to increase with height after 17:00 UTC (Figure 11b). Vertical transport of the aerosols is likely driven by surface heating, increasing near-surface temperatures and thus promoting aerosol dispersion via convection (Taylor & Jonsson, 2004; Wright et al., 2008).

For this possible event, we also evaluate the aerosol composition, following the hypothesis that the organic aerosol fraction should be high during pollen emission events. The aerosol composition shows a dominance of organic components (~48%, Figure 11c), with inorganic components contributing to rest of the total mass (NO_3^-—11%, SO_4^{2-}—32.5%, NH_4^+—8%, Cl^-—0.5%). We do not see the typical late morning peak and

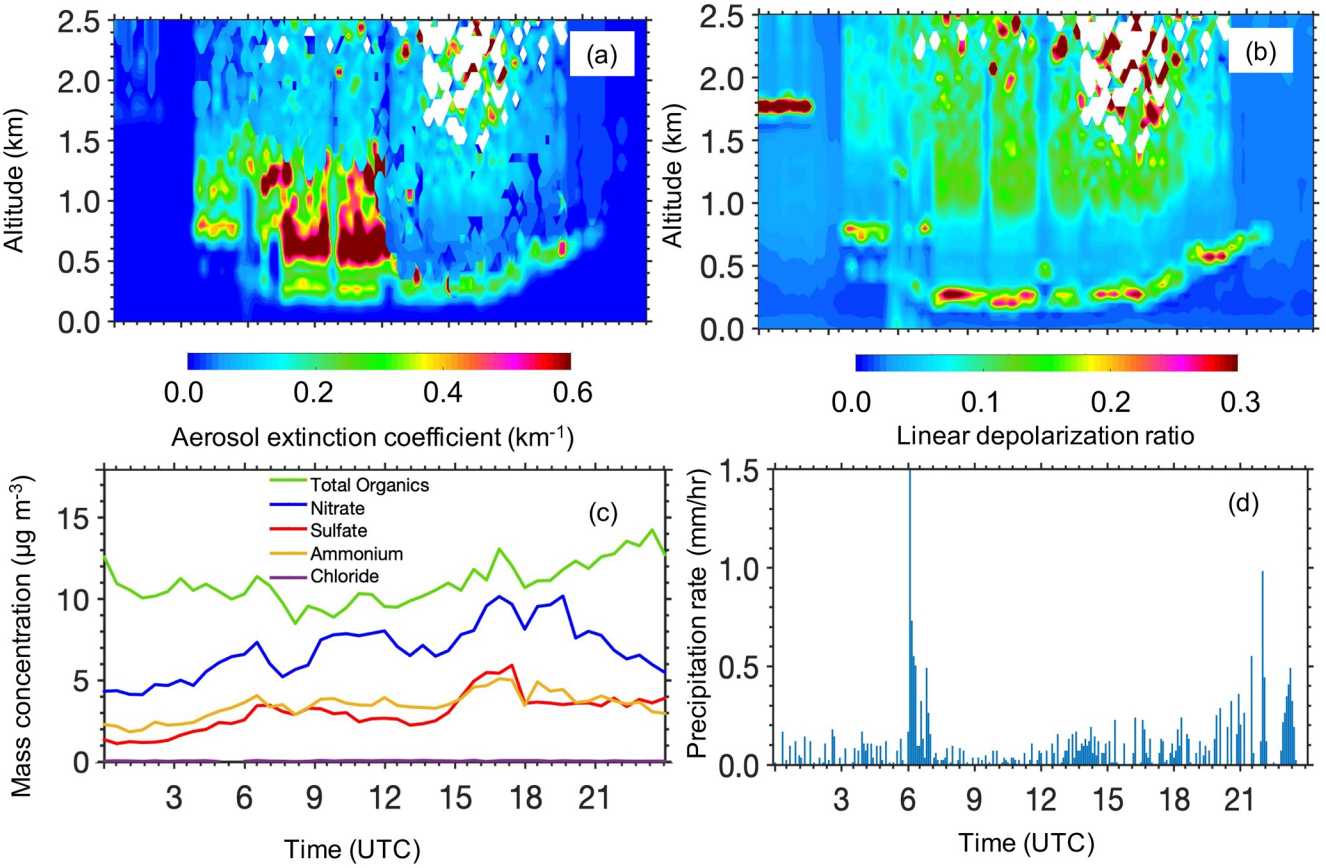

Figure 11. Selected possible pollen event (day of year [DOY] 81) in 2013. Diurnal distribution of (a) Aerosol extinction coefficient, (b) Linear depolarization ratio, (c) Particle composition mass concentration from Aerosol Chemical Speciation Monitor (ACSM) measurements and (d) Rainfall rate from rain gauge measurements at Southern Great Plains (SGP) Atmospheric Radiation Measurements (ARM) site for the event period.

afternoon decrease of the total organic particle mass concentration during this day like that of the earlier reported pollen emission days (Jones & Harrison, 2004). Pollen can be highly influenced by the local meteorology, with the rainfall playing an important role in this rupture events (Figure 11d). The high rainfall during 06:00–07:00 UTC lowers the aerosol loading (Figures 11a and 11b), with a reduction in the mass concentrations of the aerosol components. After this first rainfall event, the aerosol loading starts to accumulate with minimal precipitation from 08:00 to 19:00 UTC. A secondary peak of the rainfall during 20:00–22:00 UTC coincides with the lowering of the aerosol components other than the total organics, which appears to remove some of the particles, yet the continued high concentration of organics suggests the possibility for pollen rupture and the formation of SPPs due to their prolonged exposure to the rainfall.

4.2. Fungal Spore Rupture Event Detection

Because there have not been methods to quantify the use of depolarization ratios for fungal spore emissions, we do not have sufficient information to estimate primary fungal spore emission events as the pollen emission events (Section 4.1). Therefore, we focus on the estimation of possible fungal spore rupture events to understand the frequency of this type of biological particle event as these have been estimated previously at the site (Lawler et al., 2020).

To estimate possible fungal spore rupture events (PFE), we use the daily merged aerosol size distribution to estimate days with higher aerosol concentrations in the 20–50-nm diameter range (Lawler et al., 2020) and organic mass fraction >70% for 2011–2013 (see Section 2.3). While the aerosol size distribution has large standard deviation from the mean, the days having the highest aerosol number concentration between 20

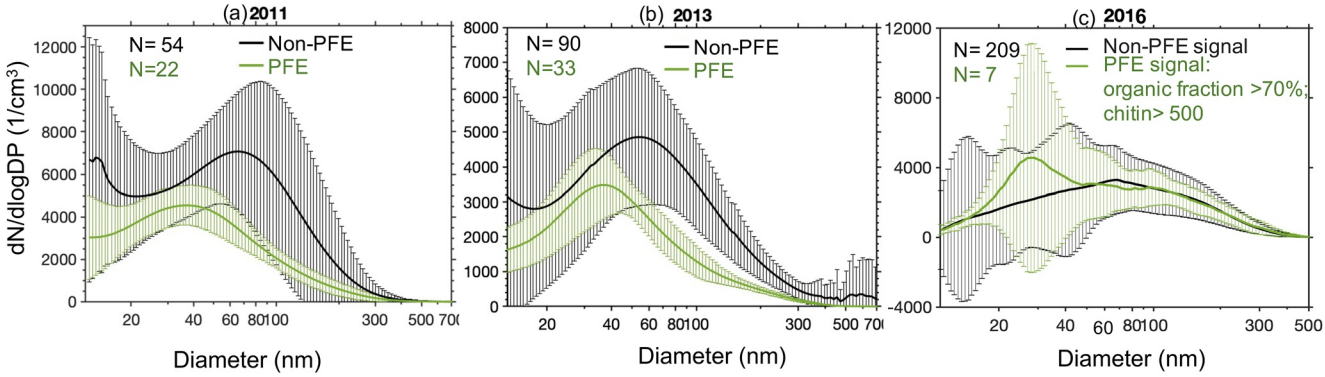

Figure 12. Daily averaged (N = number of days) merged aerosol number size distribution as a function of diameter for fungal events (higher aerosol concentrations in the 20–50-nm diameter range with organic mass fraction >70%; green) and nonfungal events (lower aerosol concentrations in the 20–50-nm diameter range with organic mass fraction >70%; black) in (a) 2011 and (b) 2013; (c) daily averaged size distributions averaged over all Thermal Desorption Chemical Ionization Mass Spectrometry (TDCIMS) negative ion mode collection periods in 2016 with total counted ions for chitin monomer ($C_8H_{12}NO_5^-$) > 500 and estimated organic mass fraction >70% for sampled ~20–50-nm particles (green), and all other TDCIMS negative ion mode collection periods (black).

and 50 nm show a lower standard deviation compared to nonevent days (Figures 12a and 12b), suggesting similar source material.

Ambient size distributions from a 2016 campaign with over 216 TDCIMS negative ion mode collection periods are also analyzed. The Aitken mode aerosol composition was measured using Thermal Desorption Chemical Ionization Mass Spectrometry (TDCIMS) at ARM SGP site during August–September 2016, as described in Lawler et al. (2020). The collected mass was assessed using a scanning mobility particle sizer (SMPS) downstream of the TDCIMS sampling filament (TSI 3025A with homemade blower/HV control). Instrument sensitivity to sulfate was calibrated using ammonium sulfate aerosol generated by atomization. Particle organic mass was estimated to be equal to the nonsulfate mass, and particle collections with low sulfate fraction and high organic fraction are less likely to be strongly influenced by particles formed by homogeneous new particle formation. In Figure 12c, the average particle size distribution when the total counted ions for chitin monomer ($C_8H_{12}NO_5^-$) exceeded 500 and estimated organic mass fraction was greater than 70% is compared to the size distribution for the remaining TDCIMS negative ion mode collection periods, effectively separating clear fungal nanoparticle signal from other time periods. From Figure 12c, the characteristic fungal fragment aerosol size distribution defined using nanoparticle chemical composition shows a peak around 20–50 nm, which is consistent with the peak in aerosol size distribution during the fungal spore rupture event days as estimated from earlier SGP data (Figures 12a and 12b).

Rainfall and humidity changes over time play an important role in fungal spore rupture events (China et al., 2016; Lawler et al., 2020). As discussed in Section 3.1, fungal spores increase during and after rain events, where rupture can occur with exposure to high humidity and rainfall for >10 h. It is kept in consideration that PFE days have an abundance of total organics and it is difficult to measure the larger fungal spores considering the lower limit of particle detection in aerosol compositional analysis instrument (Section 2). Also, as discussed in Section 4.1, the available days of the particle counts beyond the particle size range of 1 μm is very small and possible primary fungal events within 1–10 μm could not be detected.

Following the criteria for PFE events outlined in Section 3.2, we estimate up to 7% of the total number of days of observations in 2011–2013 as PFE days (Figure 13), or about 15–24 days (average of 20 days) per year depending on the conditions. Most of these days fall within the fungal peak period based on observations (Figure 3).

We note that these PFEs are short-lived and last from a few minutes to a few hours. PFE events occur within the rainfall time period or after a couple of hours of rainfall. We have selected three typical examples to reflect two main characteristics of fungal spore rupture events (Figure 14) duration of event and rainfall. The first two events (November 19, 2013; Figure 14a and November 03, 2013; Figure 14b) illustrate the range of the PFE time period, i.e., ~7 and 2 h, respectively. Both of these days exhibit high aerosol number concentrations and the diameter range that can estimate fungal spore rupture (20–50 nm; Figures 14e and 14f) and

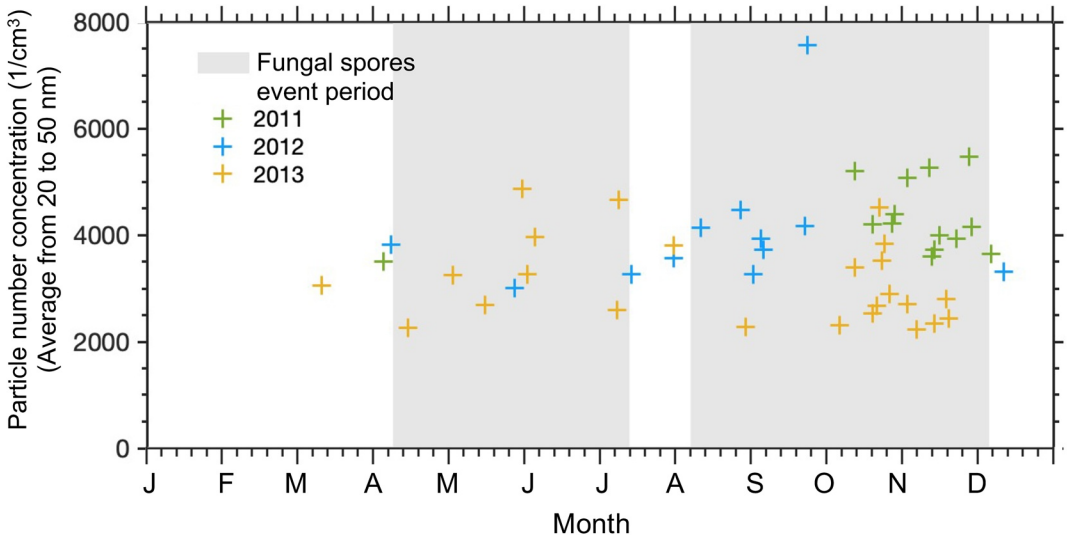

Figure 13. Annual distribution of days estimated as the possible fungal spore rupture event days. Colored crosses show the averaged particle number concentration (within the diameter range 20–50 nm) in each year, and the gray background indicates the fungal spore event periods from American Academy of Allergy Asthma and Immunology (AAAAI) measurements (Figure 3).

both occur during rainfall events. In the third case (October 23, 2013; Figure 14c) the PFE occurred after a prolonged period of exposure to rainfall for >10 h.

Aerosol number concentration counts during PFEs show higher values for the diameter range of 20–50 nm, unlike non-PFEs time periods for the same day (Figures 14e–14g). These results are consistent with the results obtained by Lawler et al. (2020) at SGP site. For contrast, we also show a non-PFE day that lacks particles number concentration peak in the diameter range from 20 to 50 nm alone (Figures 14d–14h). This day has a low rainfall intensity, showing gradual decline of the particle number concentration as the diameter range increases, with highest number concentration in the small diameter range (<20 nm). This shows an event close to a typical "banana-shaped" pattern during new particle formation event (Kalivitis et al., 2019), where there is a sudden burst and the particles show gradual growth unlike the previous examples during PFE days.

5. Conclusions

We utilize the suite of extensive aerosol measurements at the SGP DoE ARM observation site to understand the probability of occurrence of primary biological particle emission and rupture events, including both emissions and rupture for pollen as well as fungal spore rupture events for the period 2011–2015.

The long-term (2003–2010) daily pollen and fungal spores count data are obtained from the AAAAI network based closest available stations to that of the SGP ARM DoE site. For pollen, measurements at two sites in Oklahoma City and Tulsa show two distinct time periods with high total pollen counts, i.e., late winter/early spring (DOY 50–120) and late summer (DOY 240–310). For fungal spores, local counts at Tulsa suggest two distinct time periods with high total fungal spores counts, that is, late spring/early summer (DOY 110–195) and late summer/autumn (DOY 220–340). These measurements are used to estimate the likelihood of the occurrence of possible PBAP event days found using the "total aerosol" properties and the meteorological database. It is not possible to directly determine larger particle primary emissions (e.g., >1 μm) from the size distribution data due to instrument limitations; therefore, AAAAI data are generally used to classify the primary emission periods. However, ancillary data from the SGP site including chemical composition, the linear depolarization ratio, and smaller size particle distributions to estimate rupture events can provide some indication of the possible for biological particle events.

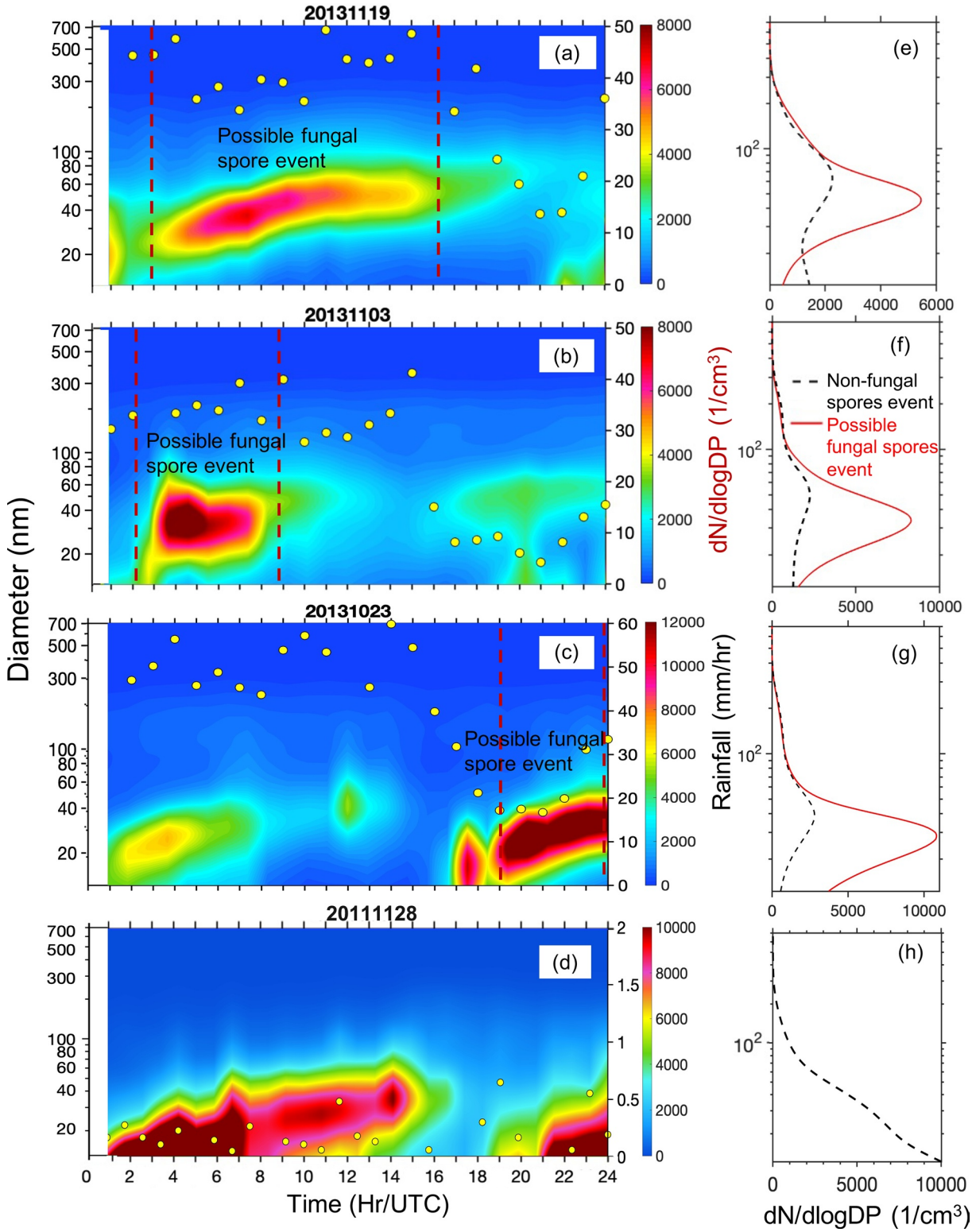

Figure 14. (a–d) The diurnal distribution of aerosol number size distribution (dN/dlnDp, in color shading) as a function of diameter (left axis) for three selected days with possible fungal spore rupture events (PFE; November 19, 2013, November 03, 2013, and October 23, 2013) and a non-PFE day (November 28, 2011). Yellow circles represent hourly rainfall (right axis). Vertical red dashed lines mark the possible fungal spore event (PFE) time period. Averaged aerosol number size distribution for the respective days (e–h) with red and black lines representing the PFE and non-PFE time period of each day, respectively.

Because most primary biological aerosol particles are larger than the particle sizes measured by the existing in-situ instrument, we are unable to use particle size alone to estimate the primary emissions of pollen and fungal spores. We estimate possible pollen emission events by (a) segregation of the days having near-surface linear depolarization ratios >0.1 provided the PPE days, (b) dominant organics fraction as compared to inorganic fractions, (c) size distribution data, and (d) diurnal patterns of size and altitude that are consistent with surface emissions. Overall, 4–19 days per year were selected as PPE days, most of which fall during the primary late winter/early spring pollination period. To estimate rupture events, daily merged aerosol size distribution data are used to estimate days with high concentration of aerosols within the size range <1 μm that occur during or after prolonged exposure of rainfall. These days were estimated as the possible pollen rupture event days which is generally known to be triggered by rainfall, while emitting the subpollen particles into the atmosphere. We further estimate possible fungal spore rupture (PFE) which met criteria similar to that of pollen ruptures, including (a) a peak of particles in the 20–50-nm size range, (b) a depletion of larger (70–300 nm) and smaller (<15 nm) particles, (c) occurrence during or after rain events, and (d) an abundance of total aerosol organics. Overall ∼7% of the days are determined as PFE days.

We note that there are substantial uncertainties in the estimation of biological aerosol emission and rupture events. Currently, most ground-based observations sites do not have adequate instrumentation to estimate pollen and fungal spores, nor do we have sufficient information on their optical and chemical properties. Growing interest in PBAP and its contribution to the atmospheric aerosol loading will require the implementation of other aerosol measurement techniques, including fluorescence, breakdown, and Raman spectroscopy; elastic scattering microscopy and holography; mass spectrometry; microfluid, paired aqueous, and remote sensing techniques (Huffman et al., 2020). Future measurements including larger size distributions, more detailed chemical composition as in Lawler et al. (2020) on longer time scales, and aerosol fluorescence measurements would be helpful to improve uncertainties on the frequency on these measurements.

Despite these limitations, here, we provide a first attempt to use long-term, existing suite of the combined aerosol and meteorological measurements to provide an estimate of the frequency of possible occurrence of biological aerosols. Overall, we estimate that PBAP primary emissions and rupture events occur about 32 days per year for a time period of few minutes to hours. This shows that these short-lived biological aerosols may have an important role in influencing the regional and global aerosol budget, and could be helpful for estimating the budget of organic aerosols. While the uncertainty of estimating the biological particle events is still high given the lack of measurements, this methodology serves as a proxy to quantify the days having possible climatic influence and health hazards due to biological aerosols even in the absence of their direct measurements. Future measurement campaigns with new instrumentation could constrain and refine this estimate in the future.

Data Availability Statement

Other atmospheric observations were obtained from the Atmospheric radiation Measurement (ARM) User facility, A U.S. Department of Energy (DOE) Office of Science user facility managed by the Biological and Environmental Research Program, and data are available from their website (https://www.arm.gov/data/). IMPROVE data are available from the Federal Land Manager Environmental Database (FED; http://views.cira.colostate.edu/fed).

Acknowledgments
T. Subba and A. L. Steiner were supported by the US Department of Energy's Atmospheric Science Research, an Office of Science Biological and Environmental Research Program (DE-SC0019084). Pollen and fungal spore count data were graciously provided by the National Allergy Board of the American Academy of Allergy, Asthma and Immunology sites in Oklahoma City (Warren V. Filley, MD FAAAAI, OK Allergy Asthma Clinic, Inc., Oklahoma City, OK and Martha Tarpay, MD, Allergy and Asthma Center, Oklahoma City, OK) and Tulsa (Estelle Levetin, Ph.D. FAAAAI, University of Tulsa, Tulsa, OK; and James Love Jr., MD PhD FAAAAI, Allergy Clinic of Tulsa, Tulsa, OK).

References

Andreae, M. O., & Crutzen, P. J. (1997). Atmospheric aerosols: Biogeochemical sources and role in atmospheric chemistry. *Science*, *276*(5315), 1052–1058. https://doi.org/10.1126/science.276.5315.1052

Andreae, M. O., & Rosenfeld, D. (2008). Aerosol-cloud-precipitation interactions. Part 1. The nature and sources of cloud-active aerosols. *Earth-Science Reviews*, *89*(1–2), 13–41. https://doi.org/10.1016/j.earscirev.2008.03.001

Bartnicki-Garcia, S., & Lippman, E. (1972). The bursting tendency of hyphal tips of fungi: Presumptive evidence for a delicate balance between wall synthesis and wall lysis in apical growth. *Journal of General Microbiology*, *73*(3), 487–500. https://doi.org/10.1099/00221287-73-3-487

Bauer, H., Claeys, M., Vermeylen, R., Schueller, E., Weinke, G., Berger, A., et al. (2008). Arabitol and mannitol as tracers for the quantification of airborne fungal spores Arabitol and mannitol as tracers for the quantification of airborne fungal spores. *Atmospheric EnvironmentAtmospheric Environment*, *42*(3), 588–593. https://doi.org/10.1016/j.atmosenv.2007.10.013

Bauer, H., Kasper-Giebl, A., Löflund, M., Giebl, H., Hitzenberger, R., Zibuschka, F., & Puxbaum, H. (2002). The contribution of bacteria and fungal spores to the organic carbon content of cloud water, precipitation and aerosols. *Atmospheric Research*, *64*, 109–119. https://doi.org/10.1016/S0169-8095(02)00084-4

Bauer, H., Kasper-Giebl, A., Zibuschka, F., Hitzenberger, R., Kraus, G. F., & Puxbaum, H. (2002). Determination of the carbon content of airborne fungal spores. *Analytical Chemistry*, *74*, 91–95. https://doi.org/10.1021/ac010331+

Bhoi, S., Qu, J. J., & Dasgupta, S. (2009). Multi-sensor study of aerosols from 2007 Okefenokee forest fire. *Journal of Applied Remote Sensing*, *3*, 031501. https://doi.org/10.1117/1.3078070

Bohlmann, S., Shang, X., Giannakaki, E., Filioglou, M., Saarto, A., Romakkaniemi, S., & Komppula, M. (2019). Detection and characterization of birch pollen in the atmosphere using a multiwavelength Raman polarization lidar and Hirst-type pollen sampler in Finland. *Atmospheric Chemistry and Physics*, *19*(23), 14559–14569. https://doi.org/10.5194/acp-19-14559-2019

Bourgeois, Q., Ekman, A. M. L., & Krejci, R. (2015). Aerosol transport over the Andes from the Amazon Basin to the remote Pacific Ocean: A multiyear CALIOP assessment. *Journal of Geophysical Research: Atmospheres*, *120*, 8411–8425. https://doi.org/10.1002/2015JD023254

Bozzetti, C., Daellenbach, K. R., Hueglin, C., Fermo, P., Sciare, J., Kasper-Giebl, A., et al. (2016). Size-resolved identification, characterization, and quantification of primary biological organic aerosol at a European rural site. *Environment Science and Technology*, *50*, 3425–3434. https://doi.org/10.1021/acs.est.5b05960

Budisulistiorini, S. H., Canagaratna, M. R., Croteau, P. L., Marth, W. J., Baumann, K., Edgerton, E. S., et al. (2013). Real-time continuous characterization of secondary organic aerosol derived from isoprene epoxydiols in downtown Atlanta, Georgia, using the Aerodyne aerosol chemical speciation monitor. *Environmental Science and Technology*, *47*(11), 5686–5694. https://doi.org/10.1021/es400023n

Burton, S. P., Ferrare, R. A., Hostetler, C. A., Hair, J. W., Rogers, R. R., Obland, M. D., et al. (2012). Aerosol classification using airborne high spectral resolution lidar measurements-methodology and examples. *Atmospheric Measurement Techniques*, *5*(1), 73–98. https://doi.org/10.5194/amt-5-73-2012

Chen, H., Hodshire, A. L., Ortega, J., Greenberg, J., McMurry, P. H., Carlton, A. G., et al. (2018). Vertically resolved concentration and liquid water content of atmospheric nanoparticles at the US DOE Southern Great Plains site. *Atmospheric Chemistry and Physics*, *18*, 311–326. https://doi.org/10.5194/acp-18-311-2018

China, S., Wang, B., Weis, J., Rizzo, L., Brito, J., Cirino, G. G., et al. (2016). Rupturing of biological spores as a source of secondary particles in Amazonia. *Environment Science and Technology*, *50*(22), 12179–12186. https://doi.org/10.1021/acs.est.6b02896

Cox, C. S., & Wathes, C. M. (1995). *Bioaerosols handbook*. CRC Press.

D'Amato, G., Vitale, C., D'Amato, M., Cecchi, L., Liccardi, G., Molino, A., et al. (2016). Thunderstorm-related asthma: What happens and why. *Clinical and Experimental Allergy*, *46*(3), 390–396. https://doi.org/10.1111/cea.12709

Després, V. R., Alex Huffman, J., Burrows, S. M., Hoose, C., Safatov, A. S., Buryak, G., et al. (2012). Primary biological aerosol particles in the atmosphere: A review. *Tellus Series B Chemical and Physical Meteorology*, *64*(1), 15598. https://doi.org/10.3402/tellusb.v64i0.15598

Després, V. R., Nowoisky, J. F., Klose, M., Conrad, R., Andreae, M. O., & Pöschl, U. (2007). Characterization of primary biogenic aerosol particles in urban, rural, and high-alpine air by DNA sequence and restriction fragment analysis of ribosomal RNA genes. *Biogeosciences*, *4*(6), 1127–1141. https://doi.org/10.5194/bg-4-1127-2007

Diehl, K., Quick, C., Matthias-Maser, S., Mitra, S. K., & Jaenicke, R. (2001). The ice nucleating ability of pollen part I: Laboratory studies in deposition and condensation freezing modes. *Atmospheric Research*, *58*(2), 75–87. https://doi.org/10.1016/S0169-8095(01)00091-6

Donovan, V. M., Wonkka, C. L., & Twidwell, D. (2017). Surging wildfire activity in a grassland biome. *Geophysical Research Letters*, *44*, 5986–5993. https://doi.org/10.1002/2017GL072901

Freudenthaler, V., Esselborn, M., Wiegner, M., Heese, B., Tesche, M., Ansmann, A., et al. (2009). Depolarization ratio profiling at several wavelengths in pure Saharan dust during SAMUM 2006. *Tellus B: Chemical and Physical Meteorology*, *61*, 165–179. https://doi.org/10.1111/j.1600-0889.2008.00396.x

Fröhlich-Nowoisky, J., Kampf, C. J., Weber, B., Huffman, J. A., Pöhlker, C., Andreae, M. O., et al. (2016). Bioaerosols in the Earth system: Climate, health, and ecosystem interactions. *Atmospheric Research*, *182*, 346–376. https://doi.org/10.1016/j.atmosres.2016.07.018

Giesecke, T., Fontna, S. L., van der Knaap, W. O., Pardoe, H. S., & Pidek, I. A. (2010). From early pollen trapping experiments to the pollen monitoring programme. *Vegetation History and Archaeobotany*, *19*, 247–258. https://doi.org/10.1007/s00334-010-0261-3

Giglio, L., Schroeder, W., & Justice, C. O. (2016). The collection 6 MODIS active fire detection algorithm and fire products. *Remote Sensing of Environment*, *178*, 31–41. https://doi.org/10.1016/j.rse.2016.02.054

Graham, B., Guyon, P., Maenhaut, W., Taylor, P. E., Ebert, M., Matthias-Maser, S., et al. (2003). Composition and diurnal variability of the natural Amazonian aerosol. *Journal of Geophysical Research*, *108*(D24), 4765. https://doi.org/10.1029/2003JD004049

Grote, M., Valenta, R., & Reichelt, R. (2003). Abortive pollen germination: A mechanism of allergen release in birch, alder, and hazel revealed by immunogold electron microscopy. *The Journal of Allergy and Clinical Immunology*, *111*(5), 1017–1023. https://doi.org/10.1067/mai.2003.1452

Grote, M., Vrtala, S., Niederberger, V., Wiermann, R., Valenta, R., & Reichelt, R. (2001). Release of allergen-bearing cytoplasm from hydrated pollen: A mechanism common to a variety of grass (poaceae) species revealed by electron microscopy. *The Journal of Allergy and Clinical Immunology*, *108*(1), 109–115. https://doi.org/10.1067/mai.2001.116431

Gute, E., & Abbatt, J. P. D. (2018). Oxidative processing lowers the ice nucleation activity of birch and alder pollen. *Geophysical Research Letters*, *45*, 1647–1653. https://doi.org/10.1002/2017GL076357

Haarig, M., Althausen, D., Ansmann, A., Klepel, A., Baars, H., Engelmann, R., et al. (2016). Measurement of the linear depolarization ratio of aged dust at three wavelengths (355, 532 and 1064 nm) simultaneously over Barbados. *EPJ Web of Conferences*, *119*, 18009. https://doi.org/10.1051/epjconf/201611918009

Hader, J. D., Wright, T. P., & Petters, M. D. (2014). Contribution of pollen to atmospheric ice nuclei concentrations. *Atmospheric Chemistry and Physics*, *14*, 5433–5449. https://doi.org/10.5194/acp-14-5433-2014

Hand, J. L., Schichtel, B. A., Pitchford, M., Malm, W. C., & Frank, N. H. (2012). Seasonal composition of remote and urban fine particulate matter in the United States. *Journal of Geophysical Research*, *117*, D05209. https://doi.org/10.1029/2011JD017122

He, Y., & Yi, F. (2015). Dust aerosols detected using a ground-based polarization lidar and CALIPSO over Wuhan (30.5°N, 114.4°E), China. *Advances in Meteorology*, *2015*, 536762. https://doi.org/10.1155/2015/536762

Helbig, N., Vogel, B., Vogel, H., & Fiedler, F. (2004). Numerical modeling of pollen dispersion on the regional scale. *Aerobiologia*, *3*, 3–19. https://doi.org/10.1023/B:AERO.0000022984.51588.30

Hinds, W. C. (1999). *Aerosol technology: Properties, behavior, and measurement of air-borne particles* (2nd ed.). John Wiley & Sons, Inc.

Hodshire, A. L., Lawler, M. J., Zhao, J., Ortega, J., Jen, C., Yli-Juuti, T., et al. (2016). Multiple new-particle growth pathways observed at the US DOE Southern Great Plains field site. *Atmospheric Chemistry and Physics*, *16*, 9321–9348. https://doi.org/10.5194/acp-16-9321-2016

Howard, L. E., & Levetin, E. (2014). Ambrosia pollen in Tulsa, Oklahoma: Aerobiology, trends, and forecasting model development. *Annals of Allergy, Asthma and Immunology*, *113*(6), 641–646. https://doi.org/10.1016/j.anai.2014.08.019

Huffman, J. A., Perring, A. E., Savage, N. J., Clot, B., Crouzy, B., Tummon, F., et al. (2020). Real-time sensing of bioaerosols: Review and current perspectives. *Aerosol Science and Technology*, *54*(5), 465–495. https://doi.org/10.1080/02786826.2019.1664724

Huffman, J. A., Prenni, A. J., Demott, P. J., Pöhlker, C., Mason, R. H., Robinson, N. H., et al. (2013). High concentrations of biological aerosol particles and ice nuclei during and after rain. *Atmospheric Chemistry and Physics*, *13*(13), 6151–6164. https://doi.org/10.5194/acp-13-6151-2013

Hughes, D. D., Mampage, C. B. A., Jones, L. M., Liu, Z., & Stone, E. A. (2020). Characterization of atmospheric pollen fragments during springtime thunderstorms. *Environmental Science and Technology Letters*, *7*(6), 409–414. https://doi.org/10.1021/acs.estlett.0c00213

Iannone, R., Chernoff, D. I., Pringle, A., Martin, S. T., & Bertram, A. K. (2011). The ice nucleation ability of one of the most abundant types of fungal spores found in the atmosphere. *Atmospheric Chemistry and Physics*, *11*, 1191–1201. https://doi.org/10.5194/acp-11-1191-2011

Ingold, C. T. (1999). Active liberation of reproductive units in terrestrial fungi. *Mycologist*, *13*(3), 113–116. https://doi.org/10.1016/S0269-915X(99)80040-8

IPCC. (2007). Climate change 2007: The physical science basis. In S. D. Qin, M. Manning, Z. Chen, M. Marquis, K. B. Averyt, M. Tignor, & H. L. Miller (Eds.), *Contribution of working group i to the fourth assessment report of the intergovernmental panel on climate change Solomon*. Cambridge University Press.

Jaenicke, R. (2005). Abundance of cellular material and proteins in the atmosphere. *Science*, *308*(5718), 73. https://doi.org/10.1126/science.1106335

Järvinen, E., Kemppinen, O., Nousiainen, T., Koiciok, T., Möhler, O., Leisner, T., & Schnaiter, M. (2016). Laboratory investigations of mineral dust near-backscattering depolarization ratios. *Journal of Quantitative Spectroscopy and Radiative Transfer*, *178*, 178–208. https://doi.org/10.1016/j.jqsrt.2016.02.003

Jones, A. M., & Harrison, R. M. (2004). The effects of meteorological factors on atmospheric bioaerosol concentrations—A review. *Science of the Total Environment*, *326*, 151–180. https://doi.org/10.1016/j.scitotenv.2003.11.021

Joung, Y. S., Ge, Z., & Buie, C. R. (2017). Bioaerosol generation by raindrops on soil. *Nature Communications*, *8*, 14668. https://doi.org/10.1038/ncomms14668

Kalivitis, N., Kerminen, V.-M., Kouvarakis, G., Stavroulas, I., Tzitzikalaki, E., Kalkavouras, P., et al. (2019). Formation and growth of atmospheric nanoparticles in the eastern Mediterranean: Results from long-term measurements and process simulations. *Atmospheric Chemistry and Physics*, *19*, 2671–2686. https://doi.org/10.5194/acp-19-2671-2019

Kim, S. W., Berthier, S., Raut, J. C., Chazette, P., Dulac, F., & Yoon, S. C. (2008). Validation of aerosol and cloud layer structures from the spaceborne lidar CALIOP using a ground-based lidar in Seoul, Korea. *Atmospheric Chemistry and Physics*, *8*, 3705–3720. https://doi.org/10.5194/acp-8-3705-2008

Kuparinen, A. (2006). Mechanistic models for wind dispersal. *Trends in Plant Science*, *11*, 297–301. https://doi.org/10.1016/j.tplants.2006.04.006

Kuparinen, A., Katul, G., Nathan, R., & Schurr, F. M. (2009). Increases in air temperature can promote wind-driven dispersal and spread of plants. *Proceedings of the Royal Society of London*, *276*(1670), 3081–3087. https://doi.org/10.1098/rspb.2009.0693

Lacey, J. (1996). Spore dispersal—Its role in ecology and disease: The British contribution to fungal aerobiology. *Mycological Research*, *100*(6), 641–660. https://doi.org/10.1016/S0953-7562(96)80194-8

Lau, A. P. S., Lee, A. K. Y., Chan, C. K., & Fang, M. (2006). Ergosterol as a biomarker for the quantification of the fungal biomass in atmospheric aerosols. *Atmospheric Environment*, *40*(2), 249–259. https://doi.org/10.1016/j.atmosenv.2005.09.048

Lawler, M. J., Draper, D. C., & Smith, J. N. (2020). Atmospheric fungal nanoparticle bursts. *Science Advances*, *6*(3), eaax9051. https://doi.org/10.1126/sciadv.aax9051

Lee, B. U., Kim, S. H., & Kim, S. S. (2002). Hygroscopic growth of *E. coli* and *B. subtilis* bioaerosols. *Journal of Aerosol Science*, *33*, 1721–1723. https://doi.org/10.1016/S0021-8502(02)00114-3

Lee, H. J., Jo, H. Y., Kim, S. W., Park, M. S., & Kim, C. H. (2019). Impacts of atmospheric vertical structures on transboundary aerosol transport from China to South Korea. *Scientific Reports*, *9*(1), 13040. https://doi.org/10.1038/s41598-019-49691-z

Lewis, W. H., Vinay, P., & Zenger, V. E. (1983). *Airborne and allergenic pollen of north America* (p. 254). The Johns Hopkins University Press.

Lindley, T. T., Speheger, D. A., Day, M. A., Murdoch, G. P., Smith, B. R., Nauslar, N. J., & Daily, D. C. (2019). Megafires on the Southern Great Plains. *Journal of Operational Meteorology*, *7*(12), 164–179. https://doi.org/10.15191/nwajom.2019.0712

Liu, Z., Vaughan, M. A., Winker, D. M., Kittaka, C., Kuehn, R. E., Getzewich, B. J., et al. (2009). The CALIPSO lidar cloud and aerosol discrimination: Version 2 algorithm and initial assessment of performance. *Journal of Atmospheric and Oceanic Technology*, *26*, 1198–1213. https://doi.org/10.1175/2009JTECHA1229.1

Mahura, A. G., Korsholm, U. S., Baklanov, A. A., & Rasmussen, A. (2007). Elevated birch pollen episodes in Denmark: Contributions from remote sources. *Aerobiologia*, *23*(3), 171–179. https://doi.org/10.1007/s10453-007-9061-3

Malm, W. C., Sisler, J. F., Huffman, D., Eldred, R. A., & Cahill, T. A. (1994). Spatial and seasonal trends in particle concentration and optical extinction in the United States. *Journal of Geophysical Research*, *99*(D1), 1347–1370. https://doi.org/10.1029/93JD02916

Marceau, A., Loubet, B., Andrieu, B., Durand, B., Foueillassar, X., & Huber, L. (2011). Modelling diurnal and seasonal patterns of maize pollen emission in relation to meteorological factors. *Agricultural and Forest Meteorology*, *151*(1), 11–21. https://doi.org/10.1016/j.agrformet.2010.08.012

Marinescu, P. J., Levin, E. J. T., Collins, D., Kreidenweis, S. M., & Van Den Heever, S. C. (2019). Quantifying aerosol size distributions and their temporal variability in the Southern Great Plains, USA. *Atmospheric Chemistry and Physics*, *19*(18), 11985–12006. https://doi.org/10.5194/acp-19-11985-2019

Melvin, M. (2018). *2018 National prescribed fire use survey report (Tech. Rep. 03-18)*. Coalition of Prescribed fire Councils, Inc.

Mielonen, T., Arola, A., Komppula, M., Kukkonen, J., Koskinen, J., de Leeuw, G., & Lehtinen, K. E. J. (2009). Comparison of CALIOP level 2 aerosol subtypes to aerosol types derived from AERONET inversion data. *Geophysical Research Letters*, *36*, L18804. https://doi.org/10.1029/2009GL039609

Miguel, A. G., Taylor, P. E., House, J., Glovsky, M. M., & Flagan, R. C. (2006). Meteorological influences on respirable fragment release from Chinese elm pollen. *Aerosol Science and Technology*, *40*(9), 690–696. https://doi.org/10.1080/02786820600798869

Möhler, O., DeMott, P. J., Vali, G., & Levin, Z. (2007). Microbiology and atmospheric processes: The role of biological particles in cloud physics. *Biogeosciences Discussions*, *4*(4), 2559–2591. https://doi.org/10.5194/bgd-4-2559-2007

Nathan, R., Katul, G. G., Bohrer, G., Kuparinen, A., Soons, M. B., Thompson, S. E., et al. (2011). Mechanistic models of seed dispersal by wind. *Theoretical Ecology*, *4*, 113–132. https://doi.org/10.1007/s12080-011-0115-3

Ng, N. L., Herndon, S. C., Trimborn, A., Canagaratna, M. R., Croteau, P. L., Onasch, T. B., et al. (2011). An aerosol chemical speciation monitor (ACSM) for routine Monitoring of the composition and mass concentrations of ambient aerosol. *Aerosol Science and Technology*, *45*(7), 770–794. https://doi.org/10.1080/02786826.2011.560211

Nieminen, T., Kerminen, V. M., Petäjä, T., Aalto, P., Arshinov, M., Asmi, E., et al. (2018). Global analysis of continental boundary layer new particle formation based on long-term measurements. *Atmospheric Chemistry and Physics*, *18*, 14737–14756. https://doi.org/10.5194/acp-18-14737-2018

NIFC. (2019). *National interagency fire center*. https://www.nifc.gov/fireInfo/fireInfostatslgFires.html

Noh, Y. M., Lee, H., Mueller, D., Lee, K., Shin, D., Shin, S., et al. (2013). Investigation of the diurnal pattern of the vertical distribution of pollen in the lower troposphere using LIDAR. *Atmosperic Chemistry and Physics*, *13*, 7619–7629. https://doi.org/10.5194/acp-13-7619-2013

Omar, A. H., Winker, D. M., Vaughan, M. A., Hu, Y., Trepte, C. R., Ferrare, R. A., et al. (2009). The CALIPSO automated aerosol classification and lidar ratio selection algorithm. *Journal of Atmospheric and Oceanic Technology*, *26*, 1994–2014. https://doi.org/10.1175/2009JTECHA1231.1

Parworth, C., Fast, J., Mei, F., Shippert, T., Sivaraman, C., Tilp, A., et al. (2015). Long-term measurements of submicrometer aerosol chemistry at the Southern Great Plains (SGP) using an Aerosol Chemical Speciation Monitor (ACSM). *Atmospheric Environment*, *106*, 43–55. https://doi.org/10.1016/j.atmosenv.2015.01.060

Pope, F. D. (2010). Pollen grains are efficient cloud condensation nuclei. *Environmental Research Letters*, *5*(4), 44015. https://doi.org/10.1088/1748-9326/5/4/044015

Pöschl, U. (2005). Atmospheric aerosols: Composition, transformation, climate and health effects. *Angewandte Chemie-International*, *44*, 7520–7540. https://doi.org/10.1002/anie.200501122

Pöschl, U., Martin, S. T., Sinha, B., Chen, Q., Gunthe, S. S., Huffman, J. A., et al. (2010). Rainforest aerosols as biogenic. *Science*, *1513*, 1513–1516. https://doi.org/10.1126/science.1191056

Prenni, A. J., Tobo, Y., Garcia, E., DeMott, P. J., Huffman, J. A., McCluskey, C. S., et al. (2013). The impact of rain on ice nuclei populations at a forested site in Colorado. *Geophysical Research Letters*, *40*, 227–231. https://doi.org/10.1029/2012GL053953

Pringle, A., Patek, S. N., Fischer, M., Stolze, J., & Money, N. P. (2005). The captured launch of a ballistospore. *Mycologia*, *97*(4), 866–871. https://doi.org/10.3852/mycologia.97.4.866

Pummer, B. G., Bauer, H., Bernardi, J., Bleicher, S., & Grothe, H. (2012). Suspendable macromolecules are responsible for ice nucleation activity of birch and conifer pollen. *Atmospheric Chemistry and Physics*, *12*(5), 2541–2550. https://doi.org/10.5194/acp-12-2541-2012

Rathnayake, C. M., Metwali, N., Jayarathne, T., Kettler, J., Huang, Y., Thorne, P. S., et al. (2017). Influence of rain on the abundance of bioaerosols in fine and coarse particles. *Atmospheric Chemistry and Physics*, *17*(3), 2459–2475. https://doi.org/10.5194/acp-17-2459-2017

Sassen, K. (2008). Boreal tree pollen sensed by polarization lidar: De-polarizing biogenic chaff. *Geophysical Research Letters*, *35*, L18810. https://doi.org/10.1029/2008GL035085

Schnell, R. C., & Vali, G. (1975). Freezing nuclei in marine waters. *Tellus*, *27*, 321–323. https://doi.org/10.3402/tellusa.v27i3.9911

Seinfeld, J. H., & Pandis, S. N. (2006). *Atmospheric chemistry and physics: From air pollution to climate change*. John Wiley & Sons, Inc.

Sicard, M., Izquierdo, R., Alarcón, M., Belmonte, J., Comerón, A., & Baldasano, J. M. (2016). Near surface and columnar measurements with a Micro Pulse Lidar of atmospheric pollen in Barcelona, Spain. *Atmospheric Chemistry and Physics Discussions*, *16*, 6805–6821. https://doi.org/10.5194/acp-2016-212

Sofiev, M., Siljamo, P., Ranta, H., & Rantio-Lehtimäki, A. (2006). Towards numerical forecasting of long-range air transport of birch pollen: Theoretical considerations and a feasibility study. *International Journal of Biometeorology*, *50*(6), 392–402. https://doi.org/10.1007/s00484-006-0027-x

Spracklen, D. V., & Heald, C. L. (2014). The contribution of fungal spores and bacteria to regional and global aerosol number and ice nucleation immersion freezing rates. *Atmospheric Chemistry and Physics*, *14*, 9051–9059. https://doi.org/10.5194/acp-14-9051-2014

Steiner, A. L., Brooks, S. D., Deng, C., Thornton, D. C. O., Pendleton, M. W., & Bryant, V. (2015). Pollen as atmospheric cloud condensation nuclei. *Geophysical Research Letters*, *42*, 3596–3602. https://doi.org/10.1002/2015GL064060

Steiner, J. L., Robertson, S., Teet, S., Wang, J., Wu, X., Zhou, Y., et al. (2020). Grassland wildfires in the Southern Great Plains: Monitoring ecological impacts and recovery. *Remote Sensing*, *12*(4), 619. https://doi.org/10.3390/rs12040619

Straka, H. (1975). *Pollen-undSporenkunde*. Fischer Verlag.

Sun, J., & Ariya, P. A. (2006). Atmospheric organic and bio-aerosols as cloud condensation nuclei (CCN): A review. *Atmospheric Environment*, *40*, 795–820. https://doi.org/10.1016/j.atmosenv.2005.05.052

Szyrmer, W., & Zawadzki, I. (1997). Biogenic and anthropogenic sources of ice-forming nuclei: A review. *Bulletin of the American Meteorological Society*, *78*(2), 209–228. https://doi.org/10.1175/1520-0477(1997)078<0209:BAASOI>2.0.CO;2

Tackenberg, O., Poschlod, P., & Bonn, S. (2003). Assessment of wind dispersal potential in plant species, ecological monographs. *Ecological Society of America*, *73*(2), 191–205. https://doi.org/10.1890/0012-9615(2003)073[0191:AOWDPI]2.0.CO;2

Taylor, P. E., Flagan, R., Miguel, A. G., Valenta, R., & Glovsky, M. M. (2004). Birch pollen rupture and the release of aerosols of respirable allergens. *Clinical and Experimental Allergy*, *34*, 1591–1596. https://doi.org/10.1111/j.1365-2222.2004.02078.x

Taylor, P. E., Flagan, R. C., Valenta, R., & Glovsky, M. M. (2002). Release of allergens as respirable aerosols: A link between grass pollen and asthma. *The Journal of Allergy and Clinical Immunology*, *109*(1), 51–56. https://doi.org/10.1067/mai.2002.120759

Taylor, P. E., & Jonsson, H. (2004). Thunderstorm asthma. *Current Allergy and Asthma Reports*, *4*, 409–413. https://doi.org/10.1007/s11882-004-0092-3

Thorsen, T. J., & Fu, Q. (2015). Automated retrieval of cloud and aerosol properties from the ARM Raman Lidar. Part II: Extinction. *Journal of Atmospheric and Oceanic Technology*, *32*(11), 1999–2023. https://doi.org/10.1175/JTECH-D-14-00178.1

Thorsen, T. J., Fu, Q., Newsom, R. K., Turner, D. D., & Comstock, J. M. (2015). Automated retrieval of cloud and aerosol properties from the ARM Raman Lidar. Part I: Feature detection. *Journal of Atmospheric and Oceanic Technology*, *32*(11), 1977–1998. https://doi.org/10.1175/JTECH-D-14-00150.1

Vali, G., DeMott, P. J., Möhler, O., & Whale, T. F. (2015). Technical note: A proposal for ice nucleation terminology. *Atmospheric Chemistry and Physics*, *15*, 10263–10270. https://doi.org/10.5194/acp-15-10263-2015

Veriankaitė, L., Siljamo, P., Sofiev, M., Šaulienė, I., & Kukkonen, J. (2010). Modeling analysis of source regions of long-range transported birch pollen that influences allergenic seasons in Lithuania. *Aerobiologia*, *26*, 47–62. https://doi.org/10.1007/s10453-009-9142-6

Wang, B., Harder, T. H., Kelly, S. T., Piens, D. S., China, S., Kovarik, L., et al. (2016). Airborne soil organic particles generated by precipitation. *Nature Geoscience*, *9*(6), 433–437. https://doi.org/10.1038/ngeo2705

Winker, D. M., Hunt, W. H., & McGill, M. J. (2007). Initial performance assessment of CALIOP. *Geophysical Research Letters*, *34*, L19803. https://doi.org/10.1029/2007GL030135

Wozniak, M. C., & Steiner, A. L. (2017). A prognostic pollen emissions model for climate models (PECM1.0). *Geoscientific Model Development*, *10*, 4105–4127. https://doi.org/10.5194/gmd-10-4105-2017

Wozniak, M. C., Steiner, A. L., & Solmon, F. (2018). Pollen rupture and its impact on precipitation in clean continental conditions. *Geophysical Research Letters*, *45*, 7156–7164. https://doi.org/10.1029/2018GL077692

Wright, S. J., Trakhtenbrot, A., Bohrer, G., Detto, M., Katul, G. G., Horvitz, N., et al. (2008). Understanding strategies for seed dispersal by wind under contrasting atmospheric conditions. *Proceedings of the National Academy of Sciences of the United States of America*, *105*(49), 19084–19089. https://doi.org/10.1073/pnas.0802697105

Zhang, Q., Jimenez, J. L., Worsnop, D. R., & Canagaratna, M. (2007). A case study of urban particle acidity and its influence on secondary organic aerosol. *Environmental Science and Technology*, *41*(9), 3213–3219. https://doi.org/10.1021/es061812j

Zhang, R., Duhl, T., Salam, M. T., House, J. M., Flagan, R. C., Avol, E. L., et al. (2014). Development of a regional-scale pollen emission and transport modeling framework for investigating the impact of climate change on allergic airway disease. *Change on Allergic Airway Disease*, *10*(3), 3977–4023. https://doi.org/10.5194/bgd-10-3977-2013

Zhang, T., Engling, G., Chan, C. Y., Zhang, Y. N., Zhang, Z. S., Lin, M., et al. (2010). Contribution of fungal spores to particulate matter in a tropical rainforest. *Environmental Research Letters*, *5*(2), 024010. https://doi.org/10.1088/1748-9326/5/2/024010

Zhu, C., Kawamura, K., & Kunwar, B. (2015). Organic tracers of primary biological aerosol particles at subtropical Okinawa Island in the western North Pacific Rim: Organic biomarkers in the north pacific. *Journal of Geophysical Research: Atmospheres*, *120*, 5504–5523. https://doi.org/10.1002/2015JD023611

Ziska, L. H. (2016). Impacts of climate change on allergen seasonality. In P. J. Beggs (Ed.), *Impacts of climate change on allergens and allergic diseases* (pp. 93–112). Cambrige University Press. https://doi.org/10.1017/CBO9781107272859